Efficacy of Suprachoroidal–Transretinal Stimulation in a Rabbit Model of Retinal Degeneration

Kentaro Nishida,[1] *Motohiro Kamei,*[1] *Mineo Kondo,*[2] *Hirokazu Sakaguchi,*[1] *Mihoko Suzuki,*[1] *Takashi Fujikado,*[1] *and Yasuo Tano*[1]

Purpose. To develop a middle-sized animal model of outer retinal degeneration and to evaluate the effectiveness of suprachoroidal–transretinal stimulation (STS) in eliciting cortical potentials from this model.

Methods. Twelve rabbits were intravenously injected with 0.47 mg/kg verteporfin and the retinas were irradiated with a red light for 90 minutes. Fluorescein angiography and full-field and focal electroretinography (ERG) were performed at 7 and 28 days after the irradiation. Electrically evoked potentials (EEPs) were elicited by electrical stimulation, with the STS electrode implanted over the irradiated region, 1 month and 1 year after the irradiation. EEPs were also recorded from three rabbits before and after retinotomy of the normal retina surrounding the degenerated area, to eliminate the influence of stray currents. The retina beneath the site of the STS electrode was examined histologically at 1 month (group 1) and 1 year (group 2) after the irradiation.

Results. An extensive area of degeneration was detected histologically, mainly in the outer retina after the irradiation. Focal ERGs were not recorded when the stimulus was confined to the irradiated area; however, EEPs were successfully elicited by STS of the same area 1 month and 1 year after the irradiation. The 360° retinectomy did not significantly alter the amplitudes, the implicit times, or the thresholds of EEPs evoked by STS.

Conclusions. Verteporfin with light irradiation induces degeneration predominantly in the outer retinal layers in rabbits. The elicitation of EEPs by STS from the degenerated area suggests that the STS system may be useful in patients with retinitis pigmentosa. (*Invest Ophthalmol Vis Sci.* 2010;51:2263–2268) DOI:10.1167/iovs.09-4120

Despite extensive attempts by genetic manipulation and artificial prosthetic devices, a practical solution for the visual decrease in patients with retinitis pigmentosa (RP) has not been obtained. Because some of the inner retinal neurons are somewhat preserved in RP patients,[1,2] several research groups are investigating whether an intraocular retinal prosthesis can restore vision in these patients by activating the functioning neurons.[3–7]

We have developed a new method of stimulating the retina called suprachoroidal-transretinal stimulation (STS),[8] and experiments on normal rabbits[9,10] and RCS rats[11] have shown that electrically evoked potentials (EEPs) can be elicited by stimulating the retina by STS. However, a middle-sized animal model with damage predominantly in the outer retinal layer, as is observed in eyes of RP patients, is needed to evaluate the effectiveness of the STS system more completely. RCS rats, S334ter rats, and P23H rats are established animal models Steinberg RH, et al. *IOVS* 1996;37:ARVO Abstract 3190)[12,13] of degeneration of the outer retinal layers, including the photoreceptors. Unfortunately, a rat eye is relatively small, which makes it difficult to implant an STS system that might be used in humans. A larger size eye model is necessary, because a safe and effective current level has not been determined in eyes of a size comparable to that of humans.

Several dog models of retinal degeneration have been identified,[14–16] but investigating a group of dogs is difficult because of the cost and labor. Thus, the purpose of this study was to develop a middle-sized animal model with predominant degeneration of the outer retinal layer which is easily available, not expensive, and easy to handle. We selected the commonly used laboratory rabbit, and induced degeneration of the outer retinal layers including the photoreceptors by photochemical damage with verteporfin. We then evaluated the efficacy of the STS system in this model.

Materials and Methods

Animals

Twelve eyes of 12 Dutch-belted rabbits (weighing 2.0–2.3 kg; Biotech, Saga, Japan) were used. All procedures conformed to the ARVO Statement for the Use of Animals in Ophthalmic and Vision Research. Every effort was made to minimize animal discomfort and to limit the number of animals to that necessary to obtain statistical significance. Nine rabbits were used for developing the retinal degeneration and the functional evaluation of the STS system; five rabbits (group 1) were used for the evaluation at 1 month, and four rabbits (group 2) were used for the evaluation at 1 year. An additional three rabbits (group 3) were used to test the validity of the model.

Light Irradiation with Verteporfin

Rabbits were anesthetized with an intramuscular injection of ketamine (33 mg/kg) and xylazine (8.5 mg/kg), and the pupils were dilated with 0.5% tropicamide and 0.5% phenylephrine hydrochloride. Verteporfin (Visudyne; Novartis, Basel, Switzerland) was injected through an ear vein at a dose of 0.47 mg/kg. This dose was determined from the results of a study of photodynamic therapy (PDT) in monkeys[17] and the results of our pilot study with 0.24, 0.47, and 0.96 mg/kg of verteporfin in rabbits. Verteporfin was reconstituted as recommended by the manufacturer.

Light irradiation was applied 5 minutes after the verteporfin infusion. A red light-emitting diode (LED; MCEP-CR8; Moritex, Tokyo, Japan) with peak emission at 630 nm was placed next to the surface of the diffuser contact lens (illuminance was 8.0×10^4 lux). The retina was irradiated from three directions—the center, nasal, and temporal

From the [1]Department of Ophthalmology, Osaka University Graduate School of Medicine, Suita, Japan; and the [2]Department of Ophthalmology, Nagoya University Graduate School of Medicine, Nagoya, Japan.

Submitted for publication June 11, 2009; revised September 18 and 28, 2009; accepted October 9, 2009.

Disclosure: **K. Nishida**, None; **M. Kamei**, None; **M. Kondo**, None; **H. Sakaguchi**, None; **M. Suzuki**, None; **T. Fujikado**, None; **Y. Tano**, None

Corresponding author: Motohiro Kamei, Department of Ophthalmology, Osaka University Graduate School of Medicine, 2-2 Yamadaoka, E7, Suita, 565-0871, Japan; mkamei@ophthal.med.osaka-u.ac.jp.

to the visual streak—with an irradiation duration of 30 minutes in each direction, which resulted in a total irradiation time of 90 minutes.

Fundus Photography and Fluorescein Angiography

Fundus photography and FA were performed with a fundus camera (TRC-50IX; Topcon, Tokyo, Japan), with the animals under general anesthesia before and at 1 month (group 1) and 1 year (group 2) after the irradiation with verteporfin. For FA, 0.075 mL/kg of 10% sodium fluorescein was injected intravenously.

Full-Field ERGs

Dark-adapted, full-field ERGs were recorded in all group 1 rabbits, 1 month after the light exposure. After 20 minutes of dark adaptation and pupil dilation, the rabbits were anesthetized with an intramuscular injection of ketamine (40 mg/kg) and xylazine (4 mg/kg), and the ERGs were picked up with a corneal Burian-Allen bipolar electrode (Hansen Ophthalmic Development Laboratories, Iowa City, IA). The rabbits were placed in a Ganzfeld bowl and stimulated with stroboscopic stimuli of 1.7 log cd-s/m^2 (photopic units). Ten responses were averaged with a stimulus interval of 10 seconds. The a-wave amplitude was measured from the baseline to the first negative trough, the b-wave from the negative trough to the positive peak.

Focal ERGs

Focal ERGs were recorded from all group 1 rabbits, 1 week and 1 month after irradiation. The techniques used for eliciting and recording focal ERGs have been described in detail.[18,19] Briefly, focal ERGs were elicited by placing the stimulus spot on the visual streak. The position of the spot on the fundus was monitored during the recording with a modified infrared fundus camera. The same Burian-Allen bipolar contact lens electrode was used to record the focal ERGs. The luminances of the stimulus and the background were 30.0 and 3.0 cd/m^2, respectively. A 5- or 30-Hz rectangular stimulus (50% on and 50% off) was used, and a 15° stimulus spot was placed on the visual streak. A total of 512 responses were averaged by a signal processor, and the time constant was 0.03 second with a 300-Hz high-cut filter.

Electrical Stimulation and Recording of EEPs at the Visual Cortex

Cortical Electrodes. With the animal under deep general anesthesia, the top of the skull was exposed and 1-mm holes were drilled through the skull 8 mm anterior to the lambdoid suture and 7 mm to the right and left of the midline. Then, screw-type stainless steel recording electrodes coated with silver, were screwed into the skull to make electrical contact with the dura mater. The reference electrode was then screwed into the skull at the bregma.

Stimulating Electrode. A single stimulating electrode was used. The wire (90% platinum, 10% iridium; diameter, 60 μm) was insulated with silicon and embedded in a 2-mm horizontal × 5.5-mm vertical × 0.1-mm-thick parylene plate. The tip of the wire was connected to a 500-μm-diameter single stimulating platinum electrode (see Fig. 3A). The inferior surface of the sclera was exposed by cutting the inferior rectus and the inferior oblique muscles. A scleral pocket (3 × 5 mm) was created just over the irradiated area on the visual streak. The electrode plate was then implanted into the scleral pocket and sutured with 5-0 Dacron onto the sclera just above the pocket. The insulated strand lead from the electrode was sutured at the limbus with 5-0 Dacron. The implanted electrode was confirmed to be located just under the damaged area of the visual streak by binocular ophthalmoscopy.

An electronic stimulator (SEN-7203; Nihon Kohden, Shinjyuku, Japan) was connected through a stimulus isolation unit (A-395R; World Precision Instruments, Sarasota, FL) to the STS electrode. The reference electrode was a platinum wire coated with polyurethane resin, and approximately 3 mm of the tip was exposed. The wire was inserted into the vitreous cavity and was fixed 1 mm posterior to the limbus with 8-0 Vicryl.

Eliciting EEPs

EEPs were recorded 1 month (groups 1 and 3) and 1 year (group 2) after irradiation. The electrical stimulating current was change from 50 to 1000 μA, and biphasic pulses were used for the electrical stimulation. The biphasic pulses consisted of current flowing from the vitreal electrode to the STS electrode in one phase and with current flowing from the STS electrode to the vitreal electrode. The duration of both phases was 0.5 ms. The threshold current for eliciting an EEP was determined by decreasing the electric current in steps. The minimum electric current that elicited the first or second positive peak of the EEP (P1 or P2) was defined as the threshold current. The EEP amplitude was measured from the baseline to the first positive trough.

Assessing Validity of This Model

To investigate the influence of stray current beyond the degenerative area where the STS stimulating electrode was placed, we removed 360° of the normal retina surrounding the degenerated area by vitrectomy and retinectomy. EEPs were recorded from the degenerated retina immediately after the retinectomy by stimulating with the STS electrode in three irradiated eyes (group 3; Figs. 3C1, 3C2). Then, EEPs were recorded before and again immediately after retinectomy in those eyes that had only the degenerated retina and optic nerve.

Histologic Study

Histologic studies were performed in the areas where the electrode was placed 1 month (group 1) and 1 year (group 2) after, to ensure that the outer retina was degenerated. After the EEPs were recorded, the stimulating electrode was removed from the eye, and the rabbits were euthanatized with a 5-mL intravenous injection of pentobarbital (50 mg/mL). The eyes were enucleated, fixed with 4% paraformaldehyde, dissected, and embedded in optimal cutting temperature compound (Tissue-Tek; Sakura Finetechnical Co. Ltd. Tokyo, Japan). Cryosections of 7-μm thickness were cut and stained with hematoxylin and eosin. The sections were examined under a light microscope and photographed with a CCD camera (AxioCam; Carl Zeiss Japan, Tokyo, Japan). The images were then analyzed (AxioVision 2.0 software for Windows; Carl Zeiss Japan). The numbers of nuclei in the outer nuclear layer (ONL), inner nuclear layer (INL), and ganglion cell layer (GCL) were counted at ×40 magnification in all eyes from groups 1 and 2. Three sections from each eye were counted; at the center of the stimulating electrode, and at ±500 μm away from the electrode. Sections were oriented along the visual streak.

Statistical Analyses

The Mann-Whitney test was used to calculate the significance of the differences in the full-field ERGs, EEPs, and cell counts between control and irradiated eyes. Paired *t*-tests were used to calculate the significance of the differences in the EEPs before and after retinectomy in group 3. $P < 0.05$ was considered statistically significant (all analyses: SigmaStat, ver.2.0; Systat, San Jose, CA).

Results

Retinal Degeneration Model

A well-defined chorioretinal atrophy was observed in all eyes by indirect ophthalmoscopy at 1 month after the irradiation. In addition, a hypofluorescent area, that corresponded to the area of the chorioretinal atrophy was seen by FA. The lesion and the hypofluorescent area remained unchanged for 1 year, whereas the area of occluded choriocapillaris increased (Figs. 1A–F).

Histologic Examination of the Retina beneath the Electrode

Photoreceptors and nuclei in the ONL were almost completely absent beneath the area where the electrode array was placed. The relative number of cells (experimental eye/control eye)

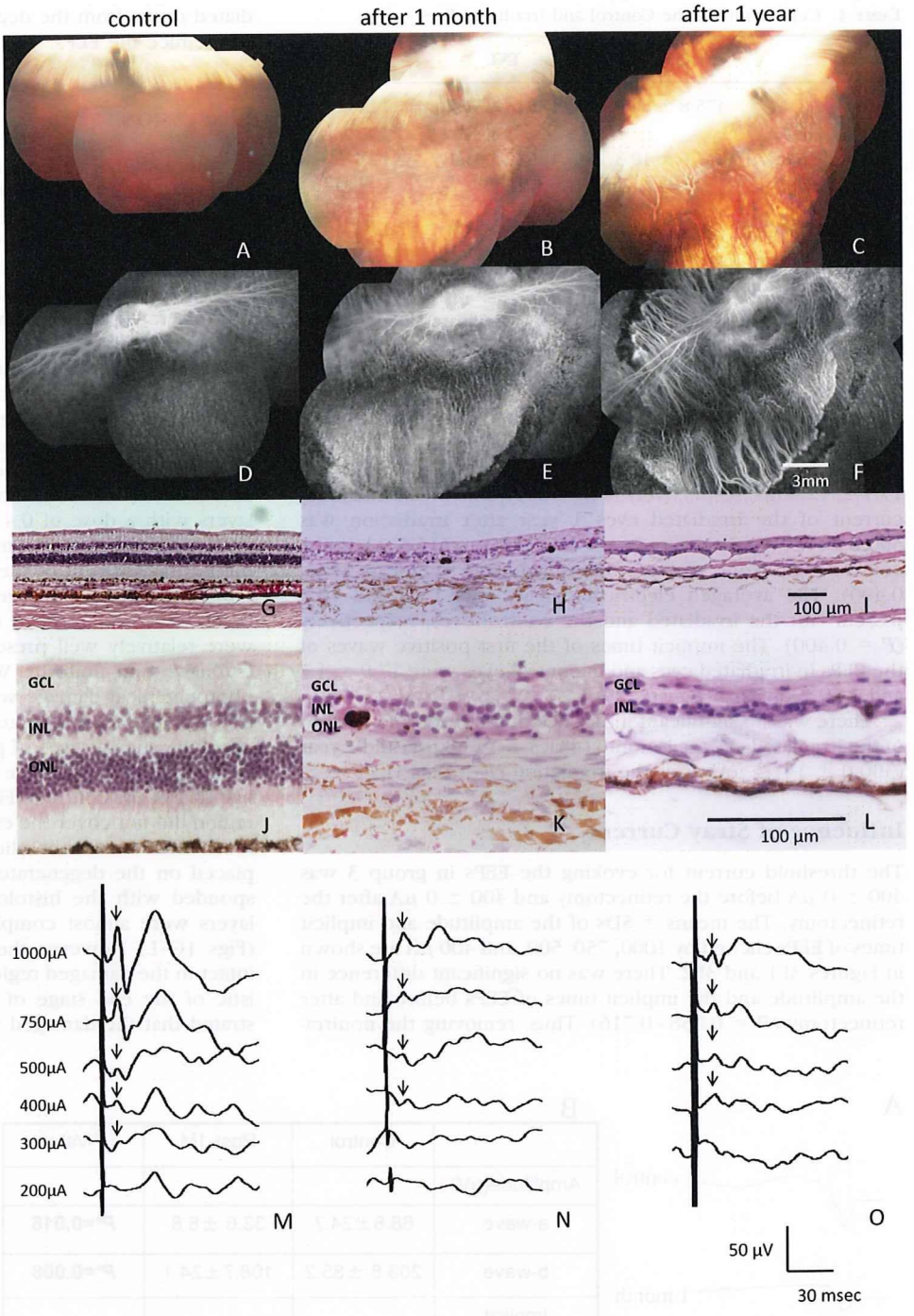

FIGURE 1. Representative fundus photographs (**A–C**), fluorescein angiograms (**D–F**), photomicrographs of the area where the electrode was placed (**G–L**), and EEPs (**M–O**) of the control and irradiated eyes at 1 month and 1 year after the irradiation with a red LED after intravenous verteporfin. (**B, C, E, F**) Atrophy of RPE and choriocapillaris can be seen. The occlusion of the choriocapillaris continued to be present at 1 year (**F**). Histopathology of the control eye (**G, J**) showed that the ONL and outer layers were fibrotic (**H, I, K, L**). At 1 year, the atrophy of the choroid had progressed, and the number of cells in the INL had decreased but the GCL was preserved (**I, L**). Scale, 100 μm. The EEPs (*arrows*) recorded after biphasic electrical pulses from the STS electrodes implanted in the control eye and degenerated eyes at 1 month and 1 year after irradiation.

was reduced to 1.5% ($P = 0.003$) in the ONL, to 56.8% ($P = 0.006$) in the INL, and to 84.5% ($P = 0.317$) in the GCL (Figs. 1G–L; Table 1). At 1 year after irradiation, the cell counts in the INL were reduced to 66% ($P = 0.004$) of the control, but those in the GCL were not significantly reduced ($P = 0.903$).

Full-Field and Focal ERGs

Representative waveforms of the dark-adapted, full-field ERGs are shown in Figure 2A, and the means ± SDs of the amplitude and implicit times of the a- and b-waves are shown in Figure 2B. We found that the amplitudes of both the a- and b-waves were reduced to about one half of the control ERGs ($P < 0.05$) at 1 month after irradiation (group 1). There was no significant difference in the implicit times of the a- and b-waves before and after the irradiation ($P = 0.548$ and $P = 0.095$).

We then recorded focal ERGs to examine the retinal function in the irradiated area. We could not record any responses with the stimulus spot placed on the irradiated area from all the eyes. The amplitudes of focal ERGs were less than the noise level (0.3 μV) for all rabbits (Fig. 2C), whereas focal ERGs with both 5- and 30-Hz stimuli from all the control eyes were recorded.

Evaluation of STS

EEPs were successfully elicited by STS from all eyes in all groups (Figs. 1M–O, 3D, 3E). The mean threshold current evoking the EEP in the irradiated eyes at 1 month after irradiation was 431.3 ± 143.8 μA and that of the control eyes was 360.0 ± 114.0 μA. This difference was not significant ($P = 0.262$). The average current density was 20.5 and 16.4 $\mu C/cm^2$

TABLE 1. Cell Counts in the Control and Irradiated Eyes

	ONL	INL	GCL
Control	475.8 ± 84.9	186.0 ± 31.2	14.8 ± 3.9
1 Month after irradiation	7.0 ± 10.3	105.6 ± 31.1	12.5 ± 3.8
*P**	**0.003**	**0.006**	0.317
1 Year after irradiation	0	69.3 ± 32.4	14.4 ± 3.3
*P**	**0.004**	**0.004**	0.903

Data are expressed as the mean ± SD.
* Mann-Whitney Rank Sum Test with significant differences in bold.

for the irradiated and control eyes, respectively ($P = 0.262$). The implicit times of the first positive waves of the EEPs in the irradiated eyes and in the control eyes were 13.4 ± 8.7 and 17.1 ± 12.4 ms, respectively ($P = 0.662$). The mean threshold current of the irradiated eyes 1 year after irradiation was 300.0 ± 141.4 μA (group 2) and was 233.3 ± 115.5 μA in the control eyes. None of these differences was significant ($P = 0.400$). The averaged electrical density was 13.6 and 10.6 μC/cm^2 for the irradiated and the control eyes, respectively ($P = 0.400$). The implicit times of the first positive waves of the EEPs in irradiated eyes and in control eyes were 17.9 ± 4.7 and 13.9 ± 5.9 ms ($P = 0.229$).

There was no significant difference in the threshold current of the irradiated eyes at 1 month (431.3 ± 143.8 μA) and 1 year (300.0 ± 141.4 μA) after the irradiation ($P = 0.413$).

Influence of Stray Current

The threshold current for evoking the EEPs in group 3 was 400 ± 0 μA before the retinectomy and 400 ± 0 μA after the retinectomy. The means ± SDs of the amplitude and implicit times of EEPs elicited by 1000, 750, 500, and 400 μA are shown in Figures 3F1 and 3F2. There was no significant difference in the amplitude and the implicit times of EEPs before and after retinectomy ($P = 0.058$–0.716). Thus, removing the nonirradiated retina from the degenerated retina and optic nerve did not reduce the EEPs.

DISCUSSION

In a pilot study, we irradiated eyes with stronger light and for longer durations (24 hours) without verteporfin and failed to damage large areas of the outer retinal layer. We, therefore, used verteporfin according to a report on the predominant damage of the outer retinal layer by repeated PDT.[17] We also chose a red LED for the light source because the LED light does not generate heat as easily as do other light sources, and 630 nm is the peak excitation wavelength of verteporfin.[20,21]

We then conducted another pilot study to develop a retinal degeneration model with verteporfin and a red LED. We changed the dose of verteporfin (0.24, 0.47, and 0.96 mg/kg), total irradiation time (45 and 90 minutes), irradiation direction (1 and 3 directions) and distance (0 and 15 mm), and finally succeeded in creating substantial damage to the outer retinal layers with a dose of 0.47 mg/kg verteporfin and irradiation from 3 directions for 30 minutes, each when the red LED was placed just in front of the diffuser contact lens. These conditions induced retinal degeneration in which the outer retinal layers were preferentially damaged and the inner retinal layers were relatively well preserved. In addition, the damage was extensive and uniform. We conclude that our technique of photochemical damage with verteporfin and a red LED light can produce retinal degeneration resembling the histologic characteristics of eyes of patients with RP.

The amplitudes of the full-field ERGs remained about one half that of the controls (Figs. 2A, 2B) because the degenerated region did not cover the entire retina (Figs. 1A–F). In contrast, focal ERGs were not elicited when the stimulus spot was placed on the degenerated area (Fig. 2C). This result corresponded with the histologic findings that the outer retinal layers were almost completely absent in the irradiated area (Figs. 1G–L). However, the inner retinal layers were somewhat intact in the damaged region, which is known to be characteristic of the end stage of human RP.[2] These results demonstrated that the damaged region of this model resembled the

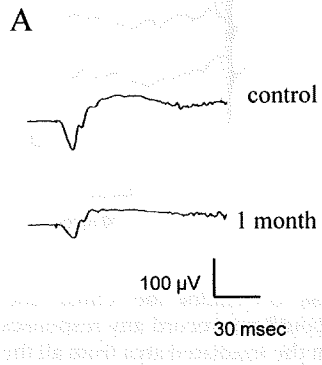

B

	Control	Post-1M	*P* Value
Amplitude(μV)			
a-wave	68.8±24.7	33.6 ±8.8	***P**=0.016*
b-wave	203.8 ±85.2	108.7±24.1	***P**=0.008*
Implicit time(ms)			
a-wave	11.2±0.6	10.7±1.2	*P**=0.548
b-wave	39.4 ±4.4	34.2±6.0	*P**=0.095

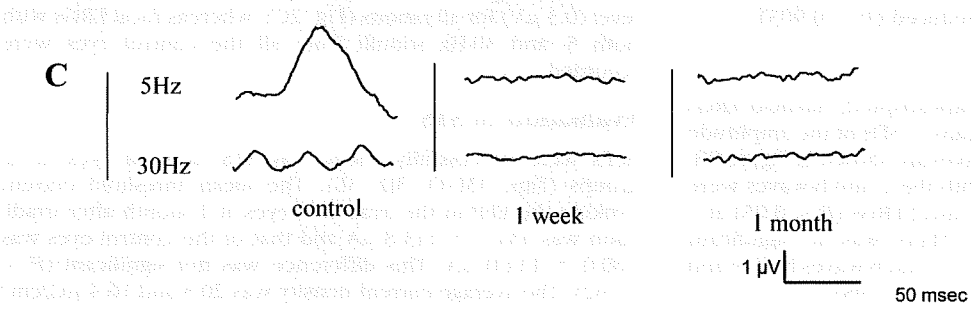

FIGURE 2. Representative full-field (A) and focal (C) ERGs at 1 month after irradiation. The amplitudes of the a- and b-waves at 1 month were reduced to one half of the control value (B). Data are shown as the means ± SD. *Mann-Whitney rank sum test with significant differences in *bold*.

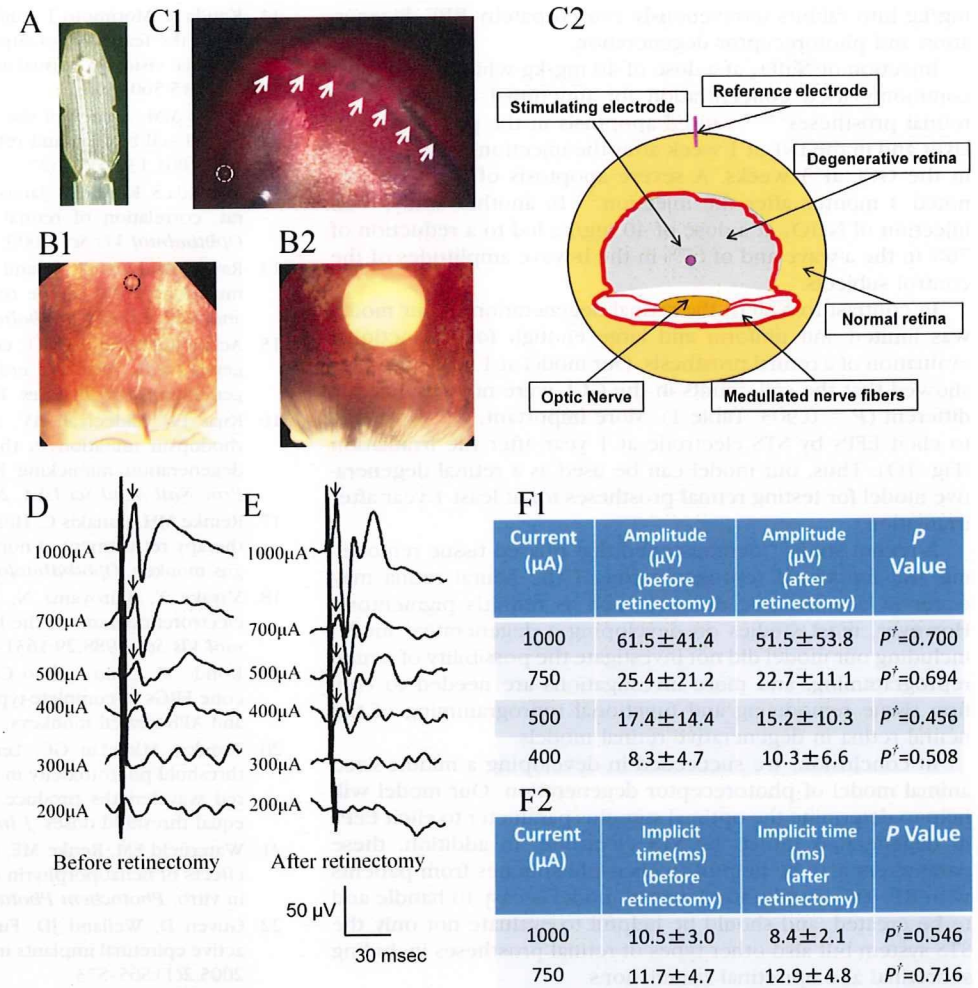

F1

Current (μA)	Amplitude (μV) (before retinectomy)	Amplitude (μV) (after retinectomy)	*P* Value
1000	61.5±41.4	51.5±53.8	$P^{\dagger}$=0.700
750	25.4±21.2	22.7±11.1	$P^{\dagger}$=0.694
500	17.4±14.4	15.2±10.3	$P^{\dagger}$=0.456
400	8.3±4.7	10.3±6.6	$P^{\dagger}$=0.508

F2

Current (μA)	Implicit time(ms) (before retinectomy)	Implicit time (ms) (after retinectomy)	*P* Value
1000	10.5±3.0	8.4±2.1	$P^{\dagger}$=0.546
750	11.7±4.7	12.9±4.8	$P^{\dagger}$=0.716
500	12.2±5.1	11.0±5.8	$P^{\dagger}$=0.339
400	14.0±5.8	11.4±6.0	$P^{\dagger}$=0.058

FIGURE 3. Inserted STS electrode and isolated degenerated retina and representative EEPs. (**A**) STS electrode (diameter 500 μm) inserted in the degenerated area (**B1**, *dotted black outline*) was apparently smaller than the photic stimuli for focal ERGs (**B2**). Retinectomy was performed (**C1**, *white arrows*) along the border of the degenerative retina and normal retina (**C2**, *red line*); inserted STS electrode (**C1**, *dotted white outline*) and representative EEPs (*black arrows*) before (**D**) and after retinectomy (**E**). The amplitudes (**F1**) and the implicit times (**F2**) of the EEPs after retinectomy were not significantly different from those before the retinectomy. Data are the mean ± SD. †Paired *t*-tests.

histologic and physiological characteristics of eyes of patients with RP.

Despite the absence of focal ERGs when the stimulus was placed on the damaged area (Fig. 2C), EEPs could still be elicited by the STS electrode placed beneath the irradiated area (Figs. 1N, 3B1, 3B2). These results indicate that the STS electrode can stimulate the inner retina in the area that has been damaged by the irradiation to evoke EEPs. One year after irradiation, the ONL had entirely disappeared, and even the INL was significantly decreased but partially remained as shown in the histologic sections (Fig. 1L, Table 1).

Because the EEPs are evoked from ganglion cells and partly from bipolar cells, even though the ONL was completely absent, the EEPs at 1 year after the irradiation were not significantly different from those recorded 1 month after the irradiation.

However, the EEPs may have been evoked by stray currents that stimulated functioning neurons some distance from the irradiated area. To eliminate this possibility, we removed the normal retina surrounding the degenerated area by retinectomy. Our findings showed that EEPs of the same amplitude and thresholds could still be elicited. Thus, we conclude that the EEPs were not elicited by stray currents (Figs. 3C–F). In addition, these findings demonstrate that the degenerated area with our parameters of photocoagulation was large enough to evaluate the effect of the STS system.

The shapes of the EEPs in our rabbits were different from those of RCD1,[22,23] which may be because of the differences in retinal prosthesis, the number of stimulating electrodes, and the current densities.

Earlier studies[24–33] reported that an intravenous administration of either monoiodoacetic acid (IAA) or sodium iodate ($NaIO_3$) can damage the retina. IAA is well known to be retinotoxic and to damage the photoreceptors selectively,[25–27] and the damage of the inner retinal layer is much less severe than that of the outer retinal layers.[24,28] However, the effect of this toxin is uneven among individuals and occasionally even between the eyes of the same animal.[28] Liang et al.[28] injected IAA intravenously at a dose of 20 mg/kg into 23 rabbits and found a uniformly decreased ONL in only 3 eyes, partial damage of the ONL in 9 eyes, and no change in 11 (48%) eyes. Because a dose of 20 mg/kg IAA is relatively high and results in a high mortality (20%),[29] increasing the dose of this drug to damage the ONL more uniformly is not practical. Our method has the advantages that a predominant outer retinal degeneration can be created with almost 100% certainty.

There are many reports[30–33] on the $NaIO_3$-induced retinal degeneration. Sorsby[31] injected different concentrations of $NaIO_3$ (10–60 mg/kg) into rabbits intravenously and concluded that an incidence of 100% of retinal lesions was attained at a dose of 25 mg/kg. But he did not evaluate the size of the lesions. In another study[32] an injection of $NaIO_3$ at a dose of 25

mg/kg into rabbits intravenously caused patchy RPE degeneration and photoreceptor degeneration.

Injection of $NaIO_3$ at a dose of 40 mg/kg which is the most commonly used concentration for functional evaluations of retinal prostheses[24,33] caused apoptosis in the photoreceptor layer and in the INL at 1 week after the injection and apoptosis in the GCL at 3 weeks. A severe apoptosis of the GCL was noted 4 months after the injection.[33] In another study,[24] an injection of $NaIO_3$ at a dose of 40 mg/kg led to a reduction of 76% in the a-wave and of 67% in the b-wave amplitudes of the control subjects.

In contrast to $NaIO_3$, the retinal degeneration of our model was limited and uniform and large enough for a functional evaluation of a retinal prosthesis. Our model at 1 year (group 2) showed that the cell counts in the GCL were not significantly different ($P = 0.903$; Table 1). More important, we were able to elicit EEPs by STS electrode at 1 year after the irradiation (Fig. 1O). Thus, our model can be used as a retinal degenerative model for testing retinal prostheses for at least 1 year after irradiation.

A recent study[34] demonstrated that phased tissue remodeling and functional reprogramming of the neural retina may occur in degenerative diseases such as retinitis pigmentosa. However, most studies on developing a degenerative model including our model did not investigate the possibility of neural reprogramming, and more investigations are needed to confirm tissue remodeling and functional reprogramming of the neural retina in degenerative retinal models.

In conclusion, we succeeded in developing a middle-sized animal model of photoreceptor degeneration. Our model will help to determine the optimal stimulus parameter to elicit EEPs in degenerated retinas by STS electrode. In addition, these parameters may be helpful to elicit phosphenes from patients with RP. This middle-sized animal model is easy to handle and to be created, and should be helpful to evaluate not only the STS system but also other types of retinal prostheses including subretinal and epiretinal stimulations.

References

1. Stone JL, Barlow WE, Humayun MS, et al. Morphometric analysis of macular photoreceptors and ganglion cells in retinas with retinitis pigmentosa. *Arch Ophthalmol.* 1992;110:1634-1639.
2. Santos A, Humayun MS, de Juan E Jr, et al. Preservation of the inner retina in retinitis pigmentosa: a morphometric analysis. *Arch Ophthalmol.* 1997;115:511-515.
3. Chow AY, Chow VY, Packo KH, at al. The artificial silicon retina microchip for the treatment of vision loss from retinitis pigmentosa. *Arch Ophthalmol.* 2004;122:460-469.
4. Humayun MS, Weiland JD, Fujii GY, et al. Visual perception in a blind subject with a chronic microelectronic retinal prosthesis. *Vision Res.* 2003;43:2573-2581.
5. Rizzo JF 3rd, Wyatt J, Loewenstein J, et al. Methods and perceptual thresholds for short-term electrical stimulation of human retina with microelectrode arrays. *Invest Ophthalmol Vis Sci.* 2003;44:5355-5361.
6. Zrenner E. The subretinal implant: can microphotodiode arrays replace degenerated retinal photoreceptors to restore vision? *Ophthalmologica.* 2002;216(suppl 1):8-20.
7. Sakaguchi H, Kamei M, Fujikado T, et al. Artificial vision by direct optic nerve electrode (AV-DONE) implantation in a blind patient with retinitis pigmentosa. *J Artif Organs.* 2009;12(3):206-209.
8. Fujikado T, Morimoto T, Kanda H, et al. Evaluation of phosphenes elicited by extraocular stimulation in normals and by suprachoroidal-transretinal stimulation in patients with retinitis pigmentosa. *Graefes Arch Clin Exp Ophthalmol.* 2007;245:1411-1419.
9. Sakaguchi H, Fujikado T, Fang X, et al. Transretinal electrical stimulation with a suprachoroidal multichannel electrode in rabbit eyes. *Jpn J Ophthalmol.* 2004;48:256-261.
10. Nakauchi K, Fujikado T, Kanda H, et al. Transretinal electrical stimulation by an intrascleral multichannel electrode array in rabbit eyes. *Graefes Arch Clin Exp Ophthalmol.* 2005;243:169-174.
11. Kanda H, Morimoto T, Fujikado T, et al. Electrophysiological studies of the feasibility of suprachoroidal-transretinal stimulation for artificial vision in normal and RCS rats. *Invest Ophthalmol Vis Sci.* 2004;45:560-566.
12. LaVail MM. Legacy of the RCS rat: impact of a seminal study on retinal cell biology and retinal degenerative diseases. *Prog Brain Res.* 2001;131:617-627.
13. Machida S, Kondo M, Jamison JA, et al. P23H rhodopsin transgenic rat: correlation of retinal function with histopathology. *Invest Ophthalmol Vis Sci.* 2000;41:3200-3209.
14. Ray K, Baldwin VJ, Acland GM, et al. Cosegregation of codon 807 mutation of the canine rod cGMP phosphodiesterase beta gene and rcd1. *Invest Ophthalmol Vis Sci.* 1994;35:4291-4299.
15. Acland GM, Fletcher RT, Gentleman S, et al. Non-allelism of three genes (rcd1, rcd2 and erd) for early onset hereditary retinal degeneration. *Exp Eye Res.* 1989;49:983-998.
16. Kijas JW, Cideciyan AV, Aleman TS, et al. Naturally occurring rhodopsin mutation in the dog causes retinal dysfunction and degeneration mimicking human dominant retinitis pigmentosa. *Proc Natl Acad Sci USA.* 2002;99:6328-6333.
17. Reinke MH, Canakis C, Husain D, et al. Verteporfin photodynamic therapy retreatment of normal retina and choroid in the cynomolgus monkey. *Ophthalmology.* 1999;106:1915-1923.
18. Miyake Y, Shiroyama N, Ota I, et al. Oscillatory potentials in electroretinograms of the human macular region. *Invest Ophthalmol Vis Sci.* 1988;29:1631-1635.
19. Kondo M, Ueno S, Piao CH, et al. Comparison of focal macular cone ERGs in complete-type congenital stationary night blindness and APB-treated monkeys. *Vision Res.* 2008;48:273-280.
20. Tsoukas MM, Lin GC, Lee MS, et al. Predictive dosimetry for threshold phototoxicity in photodynamic therapy on normal skin: red wavelengths produce more extensive damage than blue at equal threshold doses. *J Invest Dermatol.* 1997;108:501-505.
21. Waterfield EM, Renke ME, Smits CB, et al. Wavelength-dependent effects of benzoporphyrin derivative monoacid ring A in vivo and in vitro. *Photochem Photobiol.* 1994;60:383-387.
22. Guven D, Weiland JD, Fujii G, et al. Long-term stimulation by active epiretinal implants in normal and RCD1 dogs. *J Neural Eng.* 2005;2(1):S65-S73.
23. Chen SJ, Mahadevappa M, Roizenblatt R, et al. Neural responses elicited by electrical stimulation of the retina. *Trans Am Ophthalmol Soc.* 2006;104:252-259.
24. Humayun M, Sato Y, Propst R, et al. Can potentials from the visual cortex be elicited electrically despite severe retinal degeneration and a markedly reduced electroretinogram? *Ger J Ophthalmol.* 1995;4(1):57-64.
25. Noell WK. The impairment of visual cell structure by iodoacetate. *J Cell Physiol.* 1952;40:25-55.
26. Lasansky A, Robertis E. Submicroscopic changes in visual cells of the rabbit induced by iodoacetate. *J Biophysic Biochem Cytol.* 1959;5(2):245-250.
27. Noell WK. Some animal models of retinitis pigmentosa. *Adv Exp Med Biol.* 1977;77:87-91.
28. Liang L, Katagiri Y, Franco LM, et al. Long-term cellular and regional specificity of the photoreceptor toxin, iodoacetic acid (IAA), in the rabbit retina. *Vis Neurosci.* 2008;25:167-177.
29. Orzalesi N, Calabria GA, Grignolo A. Experimental degeneration of the rabbit retina induced by iodoacetic acid: a study of the ultrastructure, the rhodopsin cycle and the uptake of 14C-labeled iodoacetic acid. *Exp Eye Res.* 1970;9(2):246-253.
30. Noell WK. Metabolic injures of the visual cell. *Am J Ophthalmol.* 1955;40(2):60-70.
31. Sorsby A. Experimental degeneration of the retina, IX: fasting as a potentiating factor. *Vision Res.* 1962;2:157-162.
32. Korte GE, Reppucci V, Henkind P. RPE destruction causes choriocapillary atrophy. *Invest Ophthalmol Vis Sci.* 1984;25:1135-1145.
33. Wang K, Li XX, Jiang YR, et al. Influential factors of thresholds for electrically evoked potentials elicited by intraorbital electrical stimulation of the optic nerve in rabbit eyes. *Vision Res.* 2007;47:3012-3024.
34. Marc RE, Jones BW, Watt CB, et al. Neural reprogramming in retinal degeneration. *Invest Ophthalmol Vis Sci.* 2007;48:3364-3371.

Experimental Eye Research 90 (2010) 285–291

Contents lists available at ScienceDirect

Experimental Eye Research

journal homepage: www.elsevier.com/locate/yexer

Optimal parameters of transcorneal electrical stimulation (TES) to be neuroprotective of axotomized RGCs in adult rats

Takeshi Morimoto [a], Tomomitsu Miyoshi [b], Hajime Sawai [b], Takashi Fujikado [c,*]

[a] Department of Ophthalmology, Osaka University Graduate School of Medicine, Japan
[b] Department of Integrative Physiology, Osaka University Graduate School of Medicine, Japan
[c] Department of Applied Visual Science, Osaka University Graduate School of Medicine, 2-2 Yamadaoka, Suita City, Osaka 565-0871, Japan

ARTICLE INFO

Article history:
Received 10 September 2009
Accepted in revised form
3 November 2009
Available online 10 November 2009

Keywords:
retinal ganglion cell
neuroprotection
electrical stimulation
optic neuropathy

ABSTRACT

We previously showed that transcorneal electrical stimulation (TES) promoted the survival of axotomized retinal ganglion cells (RGCs) of rats. However the relationship between the parameters of TES and the neuroprotective effect of TES on axotomized RGCs was unclear. In the present study, we determined whether the neuroprotective effect of TES is affected by the parameters of TES. Adult male Wistar rats received TES just after transection of the left optic nerve (ON). The pulse duration, current intensity, frequency, waveform, and numbers of sessions of the TES were changed systematically. The alterations of the retina were examined histologically seven days or fourteen days after the ON transection. The optimal neuroprotective parameters were pulse duration of 1 and 2 ms/phase ($P < 0.001$, each), current intensity of 100 and 200 μA ($P < 0.05$, each), and stimulation frequency of 1, 5, and 20 Hz ($P < 0.001$, respectively). More than 30 min of TES was necessary to have a neuroprotective effect ($P < 0.001$). Symmetric pulses without an inter-pulse interval were most effective ($P < 0.001$). Repeated TES was more neuroprotective than a single TES at 14 days after ON transection ($P < 0.001$). Our results indicate that there is a range of optimal neuroprotective parameters of TES for axotomized RGCs of rats. These values will provide a guideline for the use of TES in patients with different retinal and optic nerve diseases.

1. Introduction

Neuronal activity has a neurotrophic effect on neurons (Linden, 1994; Mennerick and Zorumski, 2000). *In vivo* and *in vitro* studies have shown that electrical stimulation (ES) or neuronal activity promotes the survival and/or neurite outgrowth of different types of neurons (Fields et al., 1990; Grumbacher-Reinert and Nicholls, 1992; Al-Majed et al., 2000a,b).

In the visual system, it has been shown *in vitro* study that ES or depolarization by KCl promotes the survival and/or neurite outgrowth of cultured retinal ganglion cells (RGCs) (Meyer-Franke et al., 1998; Shen et al., 1999; Goldberg et al., 2002). Our laboratory has shown that direct ES of a transected optic nerve (ON) in adult rats promoted the survival of the axotomized RGCs in adult rats (Morimoto et al., 2002). We also showed that transcorneal electrical stimulation (TES), which is less invasive than ES of the transected ON (ON-ES), also promoted the survival of axotomized RGCs in adult rats (Morimoto et al., 2005), and In addition, promoted the survival of photoreceptors in Royal College Surgeons rats (Morimoto et al., 2007). Miyake et al. (2007) have reported that TES immediately after crushing the ON lessened the degree of visual impairment in adult rats. In the clinic, TES has been demonstrated to improve visual function in patients with nonarteritic anterior ischemic optic neuropathy, traumatic optic neuropathy (Fujikado et al., 2006), and retinal artery occlusion (Inomata et al., 2007).

In spite of these studies, the optimal TES parameters which will result in the best neuroprotective effect and safety of the retina in the clinical situation have not been determined. There are different parameters of the TES that need to be considered, e.g., pulse duration, current intensity, frequency, duration of stimulation, waveform, and number of sessions. Different combinations of these parameters also need to be considered. There are several studies on the effect of the electrical stimulation parameters on tissue damage (Yuen et al., 1981; McCreery et al., 1990; Harnack et al., 2004; Nakauchi et al., 2007), but reports on the relationship between the ES parameters and their neuroprotective effects on injured neurons are limited (Okazaki et al., 2008).

Therefore, the purpose of this study was to determine the optimal ES parameters for the neuroprotection of axotomized RGCs. To accomplish this, we cut the ON of adult rats and stimulated the eyes with electrical pulses of different duration, current intensity,

* Corresponding author. Tel.: +81 6 6879 3940; fax: +81 6 6879 3948.
E-mail address: fujikado@ophthal.med.osaka-u.ac.jp (T. Fujikado).

0014-4835/$ – see front matter © 2009 Elsevier Ltd. All rights reserved.
doi:10.1016/j.exer.2009.11.002

frequency, duration of stimulation time, waveform, and number of TES sessions. The retinas were examined histologically to determine the effectiveness of the TES in protecting the retinal neurons.

2. Materials and methods

2.1. Experimental animals

Adult male Wistar rats (230–270 g) were obtained from SLC Japan, Inc. (Shizuoka, Japan). All experimental procedures were performed in accordance with the ARVO Statement for the Use of Animals in Ophthalmic and Vision Research and were approved by the Animal Research Committee, Osaka University Graduate School of Medicine. The animals were anesthetized with intraperitoneal pentobarbital (50 mg/kg body weight) for all surgical procedures.

2.2. Retrograde labeling of RGCs

To identify the RGCs from other retinal cells, the RGCs were retrogradely labeled with Fluorogold (FG; Fluorochrome Inc., Englewood, CO), a fluorescent tracer, before the ON transection. The anesthetized animals were held on a surgical frame with a nose clamp. Craniotomy was performed on the posterior parietal bones to expose the occipital cortex. The occipital cortex was carefully aspirated to expose the dorsal surface of the bilateral superior colliculi (SC), avoiding damage to the superior sagittal sinus and SC. A small sponge soaked in 2% FG (in 0.9% NaCl containing 10% dimethyl sulfoxide) was placed on the surface of both superior colliculi (Morimoto et al., 2002, 2005; Okazaki et al., 2008).

2.3. ON transection

Seven days after the retrograde labeling of the RGCs, the left ON was transected as described in detail elsewhere (Morimoto et al., 2002, 2005; Okazaki et al., 2008). Briefly, a skin incision was made through the left eyelid close to the superior orbital rim, and the incision was retracted to expose the globe. The superior extraocular muscles were spread apart, the ON was exposed by a longitudinal incision of the orbital retractor muscle and perineurium. The ON was transected approximately 3 mm from the posterior pole of the eye with care taken not to damage the retinal blood vessels.

2.4. Transcorneal electrical stimulation

A bipolar contact lens electrode with an inner and outer ring (Kyoto Contact, Kyoto, Japan) was used as the stimulating electrodes. The corneal surface was anesthetized by 0.4% oxybuprocaine HCl in addition to systemic anesthesia, and the contact lens electrode was placed on the cornea of the eye with the transected ON. Hydroxyethylcellulose gel (1.3%) was used to protect the cornea and for making electrical contact with the cornea.

2.5. Stimulation parameters

TES was delivered with anodic first (cornea positive) biphasic square pulses from a constant current stimulator (SEN-7203; Nihonkoden, Tokyo, Japan; Isolator, A395R; World Precision Instruments, Sarasota, FL) (Morimoto et al., 2005, 2007). The stimulus parameters were: pulse durations of 0.5, 1, 2, 3, and 5 ms/phase with 100 μA, 20 Hz, and for 60 min; current intensities of 50, 100, 200, 300 and 500 μA with 1 ms/phase, 20 Hz and for 60 min; frequencies of 0.5, 1, 5, 20, 50, and 100 Hz at 100 μA, 1 ms/phase, and for 60 min; stimulation duration of 15, 30, and 60 min at 100 μA, 1 ms/phase, and 20 Hz (Table 1).

The waveform of the TES was also changed from symmetrical, asymmetrical, and symmetrical with an inter-pulse interval of 0.5 ms or 1 ms at 100 μA, 1 ms/phase, 20 Hz, and for 60 min. In addition the effect of repeated sessions of TES of 100 μA, 1 ms/phase, 20 Hz, for 60 min on days 0, 4, 7, and 10 after the ON transection was compared with a single session of TES with the same parameters of stimulation was investigated 14 days after ON transection.

Table 1
Stimulation parameters tested in this study.

Experiment	Current intensity (μA)	Pulse duration (ms/phase)	Frequency (Hz)	Stimulation duration [min]
Pulse duration	100	0.5–5	20	60
Current intensity	50–500	1	20	60
Frequency	100	1	1–100	60
Stimulation duration	100	1	20	15–60

2.6. Quantification of RGC density

Seven or 14 days after the ON transection and TES, the animals were deeply anesthetized and perfused with 4% paraformaldehyde (PFA) in 0.1 M phosphate buffer (PB, pH 7.4). Both eyes were enucleated and small incisions were made at the dorsal pole of the eyes for retinal orientation. The eyes were stored in 4% PFA in 0.1 M PB overnight at 4 °C. The retinas were dissected from the eyes, and four radial cuts were made to flatten the retinas on a glass microscope slide.

To calculate the density of the surviving RGCs, the number of FG-labeled RGCs was counted using a fluorescence microscope (Axioskop, Carl Zeiss, Oberkochen, Germany) with UV excitation at 365 nm. The RGCs in three areas of 0.5 × 0.5 mm^2 along the naso-temporal and dorso-ventral axes (nasal, temporal, dorsal and ventral) at 1, 2 and 3 mm from the optic disc were counted using a microscanner (Sapporo Beer, Saitama, Japan). The mean density of RGCs was calculated from the number of surviving RGCs counted in the 12 areas of every retina (Morimoto et al., 2002, 2005; Okazaki et al., 2008).

2.7. Statistical analyses

Data are presented as the mean ± standard deviations (SDs) and the data were statistically analyzed using a commercial software (SigmaStat, version 3.11; Systat Software, Inc). Comparisons among the groups were made by one-way analysis of variance (ANOVA), when the equal variance test passed, and was followed by the Tukey test or by Kruskal–Wallis one-way ANOVA on ranks, when the equal variance test failed, followed by the Dunn's method. Comparisons between two groups were made by Student's t tests. The level of statistical significance was set as $P < 0.05$.

3. Results

3.1. Effect of pulse duration on neuroprotection of axotomized RGCs

The somas of the RGCs in the intact control retinas were round with the fine dots of FG in the perinuclear cytoplasm and proximal dendrites (Fig. 1A). The mean RGC density in the intact control retinas was 2357 ± 150 cells/mm^2 (mean ± SD; $n = 12$; Fig. 2A). Seven days after the ON transection and without TES, the number of FG-labeled RGCs were markedly reduced to 1290 ± 96 cells/mm^2 ($n = 8$) which is 54.7% of that of intact retinas. The RGCs were irregularly shaped and debris of dead RGCs were present (Fig. 1B). The mean RGC density in the retinas with sham electrical stimulation 7 days after ON transection, was 1221 ± 176 cells/mm^2 ($n = 6$) which was 51.8% of intact retinas. This density was not significantly different from that in the retinas with ON transection without TES, and was used as the control value to evaluate the neuroprotective effect of TES.

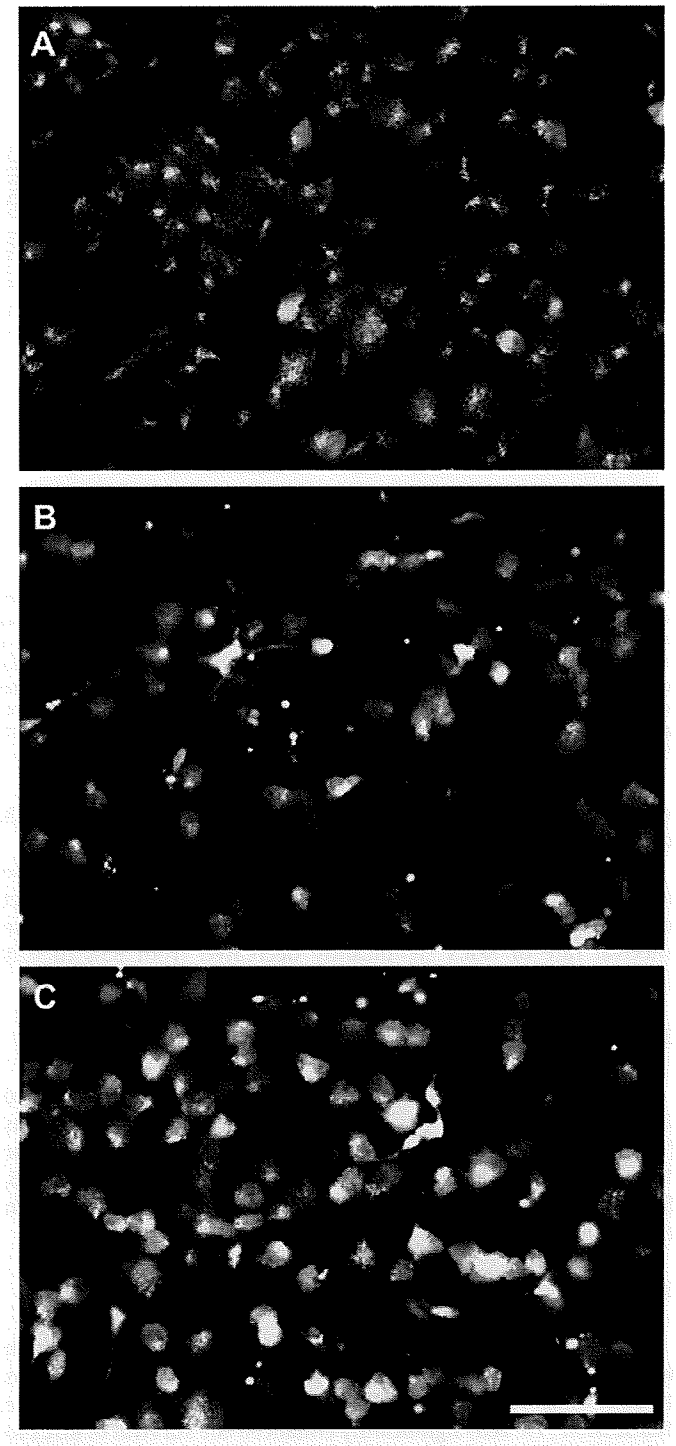

Fig. 1. Representative photographs of Fluorogold (FG)-labeled RGCs in flat-mounted retinas: intact (A), 7 days after ON transection without TES (B), ON transection with TES (C). All images were obtained from an approximately 1 mm temporal to the optic disk in each retina. A: In an intact retina, FG-labeled RGCs can be seen to have round-shaped soma with punctuate fluorescence of FG in their cytoplasm. B: In the retina 7 days after ON transection, the number of FG-labeled RGCs is markedly lower than that of RGCs in the intact retina, and debris of dead cells can be seen. C: In the retina 7 days after ON transection with TES (100 μA, 1 ms/phase, 20 Hz, 60 min), the number of surviving RGCs is strongly enhanced by TES, and many FG-labeled RGCs appeared to be similar to those in intact retinas. Scale bar = 100 μm.

Our overall results showed that TES promoted the survival of axotomized RGCs and the degree of neuroprotection depended on the pulse durations. Examination of the retinas following ON transection and TES showed many RGCs, whose shapes resembled those of the RGCs in intact retinas, had survived (Fig. 1C). The mean density of RGCs following TES of 0.5 ms/phase duration was significantly increased to 1639 ± 215 cells/mm^2 which was 69.5% of intact retinas ($P < 0.001$ vs sham stimulation; $n = 6$; Fig. 2A). TES of 1, 2 and 3 ms/phase pulse durations further increased the density up to 85.4%, 85.3% and 81.6%, respectively, of the intact retinas ($P < 0.001$; $n = 6$ each; Fig. 2A). Although TES of 5 ms/phase duration significantly increased the density of RGCs to 72.3% ($n = 6$) of that in sham stimulation, the neuroprotective effect was significantly lower than the maximum effect of 1 ms/phase ($P = 0.002$; $n = 6$; Fig. 2A).

3.2. Effect of current intensity on neuroprotection of axotomized RGCs

The mean RGC density in the retinas following TES at a current intensity of 50 μA was 1624 ± 55 cells/mm^2 ($n = 6$) which is 68.9% of intact retinas. This density was not significantly different from that in the sham stimulated retinas (Fig. 2B). However when the TES was increased to 100 μA and 200 μA, there was a significant increase in the density to 85.4% and 80.0%, respectively, of intact retinas ($P < 0.05$; $n = 6$ each). An increase of TES to 300 μA and 500 μA resulted in a decrease in the mean RGC densities to 70.0% and 64.5%, respectively, of intact retinas. These values were not significantly different from that of the sham stimulated eyes (Fig. 2B).

3.3. Effect of electric charge (intensity × duration) on neuroprotection of axotomized RGCs

The magnitude of the electric charge/phase, i.e., current intensity × pulse duration in coulombs has been identified as one of the factors that determine the effectiveness of ES in being neuroprotective in neural tissues. We compared the difference in the neuroprotective ability between increases of pulse duration to increases of current intensity. An increase in the current intensity decreased the number of RGCs more than an increase of pulse duration (Fig. 2C). There were significant differences in the number of RGCs between the survival effect with increases of current intensity and increases of pulse duration at more than 300 μC/phase ($^*P = 0.006$, $^{**}P = 0.002$; Fig. 2C).

3.4. Effect of frequency of stimulation on neuroprotection of axotomized RGCs

The mean RGC densities seven days after ON transection with sham stimulation and TES at 5 different frequencies are shown in Fig. 3. At 20 Hz, the mean RGC density was 85.0% of intact retinas which was significantly higher than that in the sham stimulated retinas ($P < 0.001$; $n = 6$). At 50 and 100 Hz, the mean RGC densities decreased to 73.1% and 68.5% respectively ($n = 6$ each), but these values were also significantly higher than that of sham stimulation. At 100 Hz the percentage of RGCs surviving after TES was significantly lower than that after 20 Hz TES ($P = 0.004$). Thus the optimal TES frequency was 20 Hz. The survival rates after TES of 5 Hz and 1 Hz were not significantly different from that at 20 Hz, 80.0% and 84.3%, respectively, of intact retinas ($n = 6$ each, $P < 0.001$ vs Sham stimulation). On the other hand, TES at 0.5 Hz did not have a significant protection, 60.8% (Fig. 3; $n = 6$).

3.5. Effect of waveform on neuroprotection of axotomized RGCs

The neuroprotective effects of the three types of waveforms with equal charge-balance were different (Fig. 4A). TES with Type II, symmetric waveforms led to a significantly increased survival of 85% compared to the sham stimulation, while asymmetrical

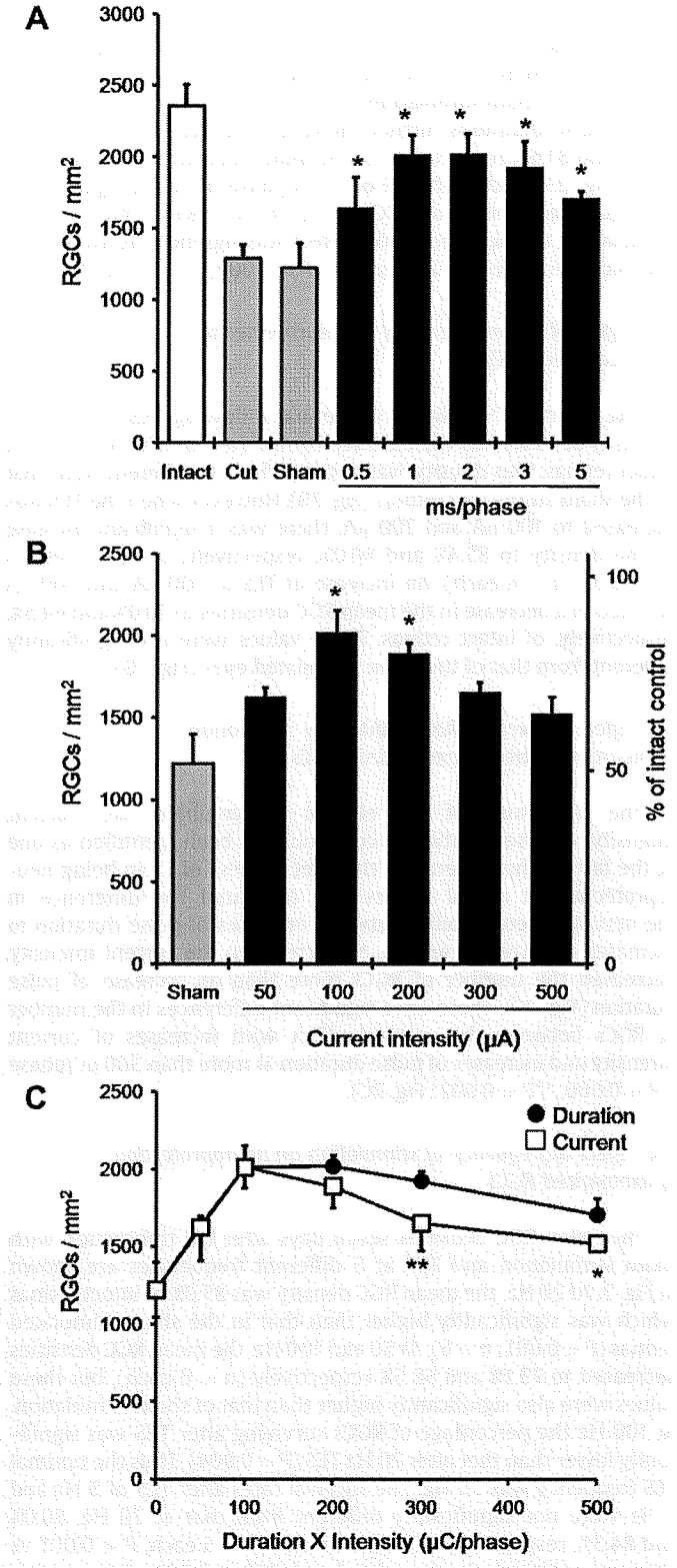

Fig. 2. Effects of pulse duration and current intensity of TES on the survival of axotomized RGCs 7 days after ON transection. A: Pulse duration-dependent neuroprotective effect of TES on RGC survival. TES (current intensity: 100 μA; frequency: 20 Hz) for 1 h was applied immediately after the ON was transected. The density of the FG-labeled RGCs/mm^2 is presented as the means ± SDs. Seven days after ON transection, the density of the RGCs is reduced to 54% of the control (Cut group). In the sham-treated animals (no electrical stimulation after ON transection), the density decreased to 53% of that of the intact control retina (Sham group). The RGC density in all five groups with TES (0.5, 1, 2, 3, and 5 ms/phase pulse duration) was significantly higher than in the sham group. Statistical analysis was made by one-way ANOVA followed by Tukey test ($P < 0.001$, *$P < 0.001$ compared with sham). B: Current intensity-dependent neuroprotective effect of TES on RGC survival 7 days after ON transection. TES (pulse duration: 1 ms/phase; frequency: 20 Hz) for 1 h was applied immediately after ON transection. TES at 100 μA and 200 μA significantly increased the mean RGC densities compared with sham stimulation. Statistical analysis was made by Kruskal–Wallis One-Way Analysis of Variance on Ranks followed by Dunn's method ($P < 0.001$, *$P < 0.05$ compared with sham). C. Comparison of neuroprotective effect of TES with pulse duration change and that with current intensity change 7 days after ON transection. The survival effect by current intensity significantly decreases as compared with that by pulse duration (more than 300 μC/phase) (t test, **$P = 0.002$, *$P = 0.006$).

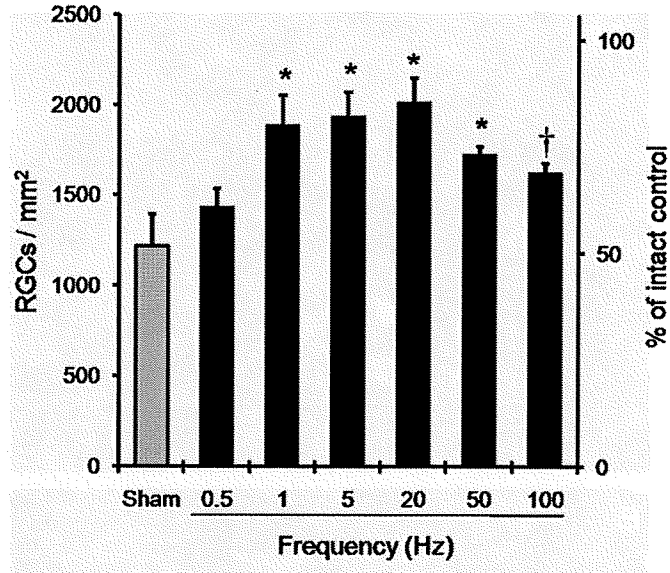

Fig. 3. Frequency-dependent neuroprotective effect of TES on axotomized RGCs 7 days after ON transection. TES (current intensity 100 μA; pulse duration 1 ms/phase) for 1 h was applied immediately after ON transection. TES at 1–20 Hz exerted the most significant effect on RGC survival; the mean densities of RGCs at 1–20 Hz exerted the most significant effect on RGC survival; the mean densities of RGCs at 1–20 Hz was significantly higher than the sham stimulation group ($P < 0.005$). Statistical analysis between the sham stimulation and ES groups was performed using one-way ANOVA followed by Tukey test ($P < 0.01$, *$P < 0.005$, †$P < 0.001$ compared with sham).

waveforms of Type I led to a survival of 68.7% and Type III to 68.3% of intact retinas ($P < 0.001$; $n = 6$ each; Fig. 4B).

Next we examined the effect of the addition of inter-pulse interval to symmetrical pulses on the survival-promoting effect on RGCs (Fig. 4C). As the inter-pulse interval was increased, the survival rate of RGCs significantly decreased from 85% to 62% ($P < 0.001$; $n = 6$ each; Fig. 4D).

3.6. Stimulation duration on neuroprotection of axotomized RGCs

TES for 30 min significantly increased the survival of RGCs to 1802 ± 111 cells/mm^2 ($n = 6$) which is 76.8% of intact retinas ($P < 0.001$ vs sham stimulation). On the other hand, after TES for 10 min, the mean RGC density was 1398 ± 124 cells/mm^2 ($n = 6$, 59.3% of intact retinas), which was not significantly different than that of the sham stimulated retinas (Fig. 5).

3.7. Effect of repeated TES on neuroprotection of axotomized RGCs

The mean RGC density in retinas 14 days after ON transection with sham stimulation was 350 ± 216 cells/mm^2 ($n = 6$), which was 13.9% of intact retinas ($n = 6$; Fig. 6A,D). On the other hand, a single TES session (1× TES) significantly enhanced the survival of RGCs to 22.9% of intact retinas ($P < 0.001$ vs sham; $n = 6$; Fig. 6B,D). Four TES sessions (4× TES on days 0, 4, 7 and 10 after ON transection) further increased the number of RGCs to 47.1% of intact retinas ($P = 0.024$ vs 1× TES; $n = 6$; Fig. 6C,D).

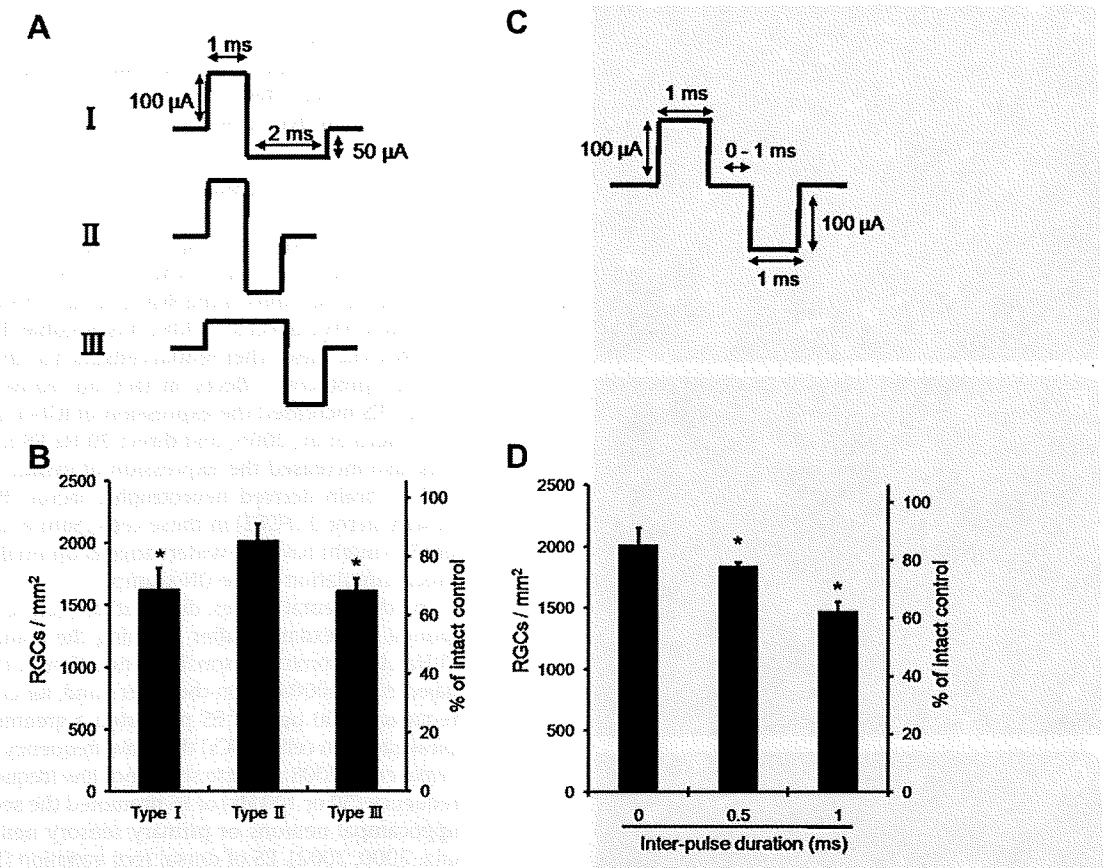

Fig. 4. Effects of waveforms of TES on the survival of axotomized RGCs 7 days after ON transection. A: Waveforms of the biphasic stimuli used in this study. Type I: Asymmetric rectangular pulse waveform (anodic first wave 100 μA, 1 ms/phase and cathodic second wave 50 μA, 2 ms/phase), Type II: Symmetric rectangular pulse waveform (100 μA, 1 ms/phase), Type III: Asymmetric rectangular pulse waveform (anodic first wave 50 μA, 2 ms/phase and cathodic second wave 100 μA, 1 ms/phase). All waves were charge-balanced. B: Neuroprotective effect of each waveform on axotomized RGCs 7 days after ON transection. TES with symmetric waveform (Type II) significantly increased the survival of RGCs more than asymmetric waveforms (Type I and Type III). Statistical analysis was performed using one-way ANOVA followed by Tukey test ($P < 0.001$, $^*P < 0.001$ compared with Type II). C: Waveform of a symmetric waveform with inter-pulse interval. D: Effect of inter-pulse interval on axotomized RGCs. The neuroprotective effect of TES on RGCs significantly decreased depending on the length of inter-pulse interval. Statistical analysis was performed using one-way ANOVA followed by Tukey test ($P < 0.001$, $^*P < 0.001$ compared with Type II without inter-pulse interval).

4. Discussion

Our results showed that the neuroprotective effect of TES on axotomized RGCs was dependent on the pulse duration, current intensity, frequency, stimulation duration, waveform, and the number of stimulation sessions.

4.1. Current charge (pulse duration × intensity)

The neuroprotective effect of TES was dependent on both the pulse duration and current intensity. There was a range of optimal pulse durations and current intensities, and an increase of the pulse duration or current intensity over the optimal range decreased the survival-promoting effect. On the other hand, the density of the electric charge, which is the production of current intensity and pulse duration, determined the extent of neural tissue damage (Yuen et al., 1981; McCreery et al., 1990; Harnack et al., 2004; Nakauchi et al., 2007). We found that there was a significant difference in neuroprotective effect of pulse duration and current intensity, on the basis of the same amount of electric charges (more than 300 μC/phase). In a retinal prosthesis study using supra-choroidal–transretinal stimulation (STS), the threshold of electric charge for the retinal safety was lower with shorter pulse durations even with the same amount of electric charge (Nakauchi et al., 2007). This is similar to our present results. Because the electric charge rate within an unit time became larger with an increase of

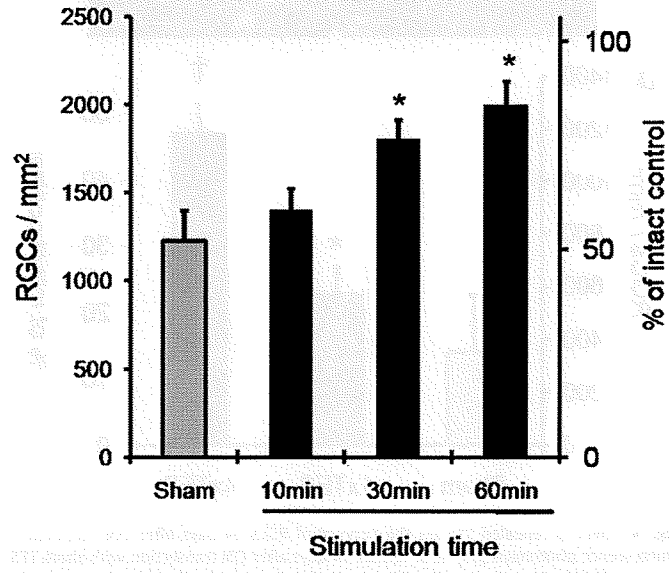

Fig. 5. Effect of stimulation duration on neuroprotection of axotomized RGCs. TES (current intensity: 100 μA; pulse duration: 1 ms/phase; frequency: 20 Hz) was applied immediately after ON transection. In the 10 min ES group, the mean density of RGCs was not significantly different from that in the sham group. In the 30 and 60 min groups, the mean density was significantly higher than that in the sham group ($P < 0.001$; each $n = 6$). Statistical analysis among the groups was performed using one-way ANOVA ($P < 0.001$) followed by Tukey test ($^*P < 0.001$ compared with the sham group).

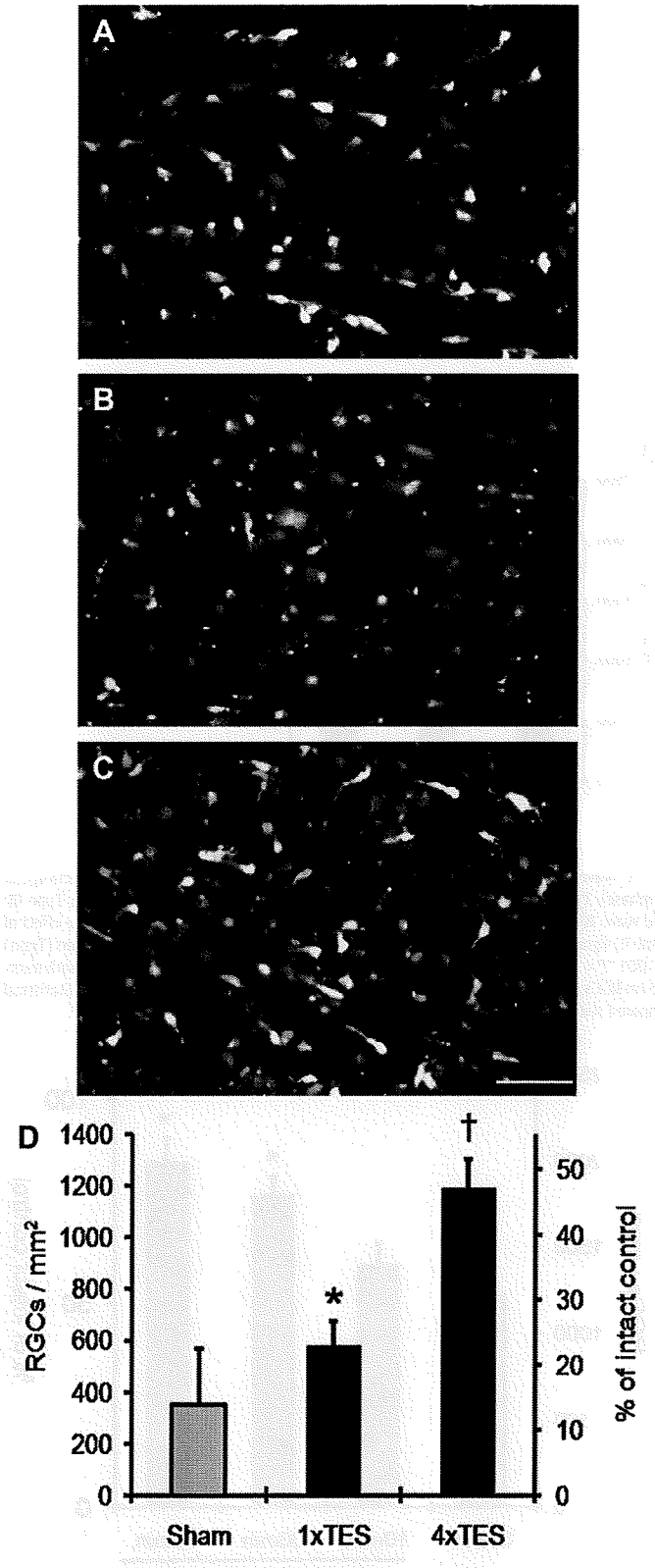

Fig. 6. Effect of repeated TES on the survival of RGCs 14 days after ON transection. Fluorescence photomicrographs of retinas 14 days after ON transection with sham TES (A), with single TES (B) and 4 times TES (C). Only a few FG-labeled RGCs are present 14 days after ON transection with sham stimulation (A). On the other hand single TES increased the viable RGCs (B), and 4× TES further increased the viable RGCs than 1× TES (C), Scale bar = 100 μm. Mean density of RGCs 14 days after ON transection with sham TES was much lower than that in the retina 7 days after ON transection. Although the mean density of RGCs 14 days after ON transection with 1× TES was also lower than that of RGCs 7 days after ON transection with TES, the density remained significantly higher than that with sham TES 14 days after ON transection ($P = 0.02$). Moreover 4× TES significantly increased the surviving RGCs more than single TES 14 days after ON transection ($P < 0.001$). One-way ANOVA: $P < 0.001$, followed by Tukey test: $^{*}P = 0.02$, $^{\dagger}P < 0.001$ comparing with sham group (D).

current intensity than with an increase of pulse duration, the increase of electric current may cause greater tissue damage even if the same amount of electric charge/phase is given. Therefore the neuroprotective effect may be lower with an increase of current intensity than that of pulse duration.

4.2. Frequency-dependent effect of TES on RGC survival

TES of 1–20 Hz frequency had the greatest neuroprotection on RGCs. On the other hand, when the ON stump is stimulated thus stimulating the axons of the RGCs, 20 Hz of ES was the most optimal frequency (Okazaki et al., 2008). It is possible that TES stimulates not only RGCs but also other retinal cells such as the Müller cells to exert its neuroprotective effects. In fact, our earlier study showed that 20 Hz TES increased the expression of IGF-1 in Müller cells *in vivo* (Morimoto et al., 2005) and direct 20 Hz ES to the cultured Müller cells also increased the expression of insulin-like growth factor-1 (IGF-1), brain derived neurotrophic factor (BDNF) and fibroblast growth factor 2 (FGF2) in these cells (Sato et al., 2008a,b,c). Therefore TES might have the wider range of optimal frequencies than the direct stimulation of the ON stump.

In other neural tissues, different frequencies were reported to be optimal. For example, after crushing the spinal cord *in vivo*, ES at 20 Hz also promoted axonal regeneration of the motoneurons (Al-Majed et al., 2000a,b). On the other hand, for cochlear implants high frequency (300 pps) of ES promoted a greater survival of ototoxic spiral ganglion cells (SGCs) than low frequency (30 pps) of ES *in vivo* (Leake et al., 2008). *In vitro* study, not low frequency (20 Hz) but high frequency (50 or 100 Hz) of ES promoted the secretion of BDNF from hippocampal neurons or primary sensory neurons (Balkowiec and Katz, 2000, 2002). ES of dorsal root ganglion (DRG) axons at 20 Hz promoted greater axonal regeneration than 200 Hz (Udina et al., 2008). Thus the optimal frequency of ES to have neuroprotective effects differs for different types of neurons and nervous systems. Because neurons and glial cells have various voltage-sensitive ion channels for each cells, the activation of ion channels may depend on the frequency of ES. For example, Müller cells have voltage-sensitive L-type Ca channel (Xu et al., 2002). We have demonstrated that 20 Hz ES activates voltage-sensitive L-type Ca channels to increase the expression of the mRNAs of IGF-1 and BDNF in cultured Müller cells (Sato et al., 2008a,b). In hippocampal neurons, 100 Hz ES activates the N-type Ca channels to make hippocampal neurons release BDNF (Brosenitsch and Katz, 2001). Another possibility is that high frequency of ES induces greater tissue damage. In the cat's sciatic nerve, ES at 100 Hz and 50 Hz cause the severe neural damage, although ES at 20 Hz induces little or no neural damage (McCreery et al., 1995). Thus it is important to select the suitable frequency of ES applied for each type of neuron.

4.3. Effect of waveforms on the TES-induced neuroprotective effect

TES with symmetric pulse waves increased the number of surviving RGCs more than TES with asymmetric pulse waves, although both pulse waves were charge-balanced. Moreover, longer inter-pulse intervals resulted in less surviving RGCs than TES with no inter-pulse intervals. It is possible that the electric charge might not be balanced well by asymmetrical pulses to cause the tissue damage. Or it is possible that the increase in the inter-pulse interval than the safety limit, might cause the tissue damage. In cochlear

implants, the threshold of auditory nerve response evoked by ES with asymmetric pulse waves is lower than that by ES with symmetric pulse waves and the threshold of auditory nerve response evoked by long inter-pulse intervals is lower than that by the ES without inter-pulse intervals (Macherey et al., 2006). The effects of asymmetrical or symmetrical pulses with long inter-pulse intervals were similar to monophasic pulses (Macherey et al., 2006). These pulses might lead to neural damage with the lower electric charge than the symmetric pulses.

4.4. Stimulation time-dependent effect of TES on RGC survival

TES for 10 min immediately after ON transection did not increase the number of surviving RGCs, but that for 30 min did. This result is similar to that following ES of the transected ON stump (Okazaki et al., 2008). These results indicate that ES to RGCs may influence the intrinsic survival signal or the death signal. It may take more than 30 min of intervention to obtain some survival signals. Further investigation is needed to determine what kind of signals are being induced.

4.5. Single TES vs repeated TES for long-lasting neuroprotection

Fourteen days after ON transection, the densities of surviving RGCs in the retinas with single TES (1× TES) were still higher than in the control retinas without TES. And repetitive TES (4× TES) increased the number of surviving RGCs more than 1× TES. These results indicate that repeated TES has cumulative neurotrophic effects on the long term survival of RGCs. In fact we have demonstrated that TES up-regulates the expression of the mRNA and protein of IGF-1 to rescue axotomized RGCs (Morimoto et al., 2005). Our results suggest that IGF-1 induced by TES might be cumulative and have neuroprotective effects of RGCs continuously for 2 weeks. The mechanism of repetitive TES on the longer term survival of RGCs should be investigated in the future.

5. Conclusions

We performed a systematic analysis of the neuroprotective effect of different stimulus parameters of TES on axotomized RGCs. We concluded that the optimal parameter of TES on the neuroprotection of RGCs are: current intensity of 100–200 μA, pulse duration of 1–3 ms/phase, frequency of 1–20 Hz, stimulation duration of 30–60 min, symmetrical pulse waves without inter-pulse intervals, and repeated stimulations. It is important that stimulation with these optimal parameters with low electric power, is applied for the overall period to maintain long term survival of RGCs. These findings should serve as guideline for ES in humans.

Acknowledgments

We thank Professor Yasuo Tano for helpful advice and various supports.

This work was supported by a Health Sciences Research Grant (H19-sensory-001) from the Ministry of Health, Labour and Welfare, Japan.

References

Al-Majed, A.A., Neumann, C.M., Brushart, T.M., Gordon, T., 2000a. Brief electrical stimulation promotes the speed and accuracy of motor axonal regeneration. J. Neurosci. 20, 2602–2608.

Al-Majed, A.A., Brushart, T.M., Gordon, T., 2000b. Electrical stimulation accelerates and increases expression of BDNF and trkB mRNA in regenerating rat femoral motoneurons. Eur. J. Neurosci. 12, 4381–4390.

Balkowiec, A., Katz, D.M., 2000. Activity-dependent release of endogenous brain-derived neurotrophic factor from primary sensory neurons detected by ELISA in situ. J. Neurosci. 20, 7417–7423.

Balkowiec, A., Katz, D.M., 2002. Cellular mechanisms regulating activity-dependent release of native brain-derived neurotrophic factor from hippocampal neurons. J. Neurosci. 22, 10399–10407.

Brosenitsch, T.A., Katz, D.M., 2001. Physiological patterns of electrical stimulation can induce neuronal gene expression by activating N-type calcium channels. J. Neurosci. 21, 2571–2579.

Fields, R.D., Neale, E.A., Nelson, P.G., 1990. Effects of patterned electrical activity on neurite outgrowth from mouse sensory neurons. J. Neurosci. 10, 2950–2964.

Fujikado, T., Morimoto, T., Matsushita, K., Shimojo, H., Okawa, Y., Tano, Y., 2006. Effect of transcorneal electrical stimulation in patients with nonarteritic ischemic optic neuropathy or traumatic optic neuropathy. Jpn. J. Ophthalmol. 50, 266–273.

Goldberg, J.L., Espinosa, J.S., Xu, Y., Davidson, N., Kovacs, G.T., Barres, B.A., 2002. Retinal ganglion cells do not extend axons by default: promotion by neurotrophic signaling and electrical activity. Neuron 33, 689–702.

Grumbacher-Reinert, S., Nicholls, J., 1992. Influence of substrate on retraction of neurites following electrical activity of leech Retzius cells in culture. J. Exp. Biol. 167, 1–14.

Harnack, D., Winter, C., Meissner, W., Reum, T., Kupsch, A., Morgenstern, R., 2004. The effects of electrode material, charge density and stimulation duration on the safety of high-frequency stimulation of the subthalamic nucleus in rats. J. Neurosci. Methods 138, 207–216.

Inomata, K., Shinoda, K., Ohde, H., Tsunoda, K., Hanazono, G., Kimura, I., Yuzawa, M., Tsubota, K., Miyake, Y., 2007. Transcorneal electrical stimulation of retina to treat longstanding retinal artery occlusion. Graefes. Arch. Clin. Exp. Ophthalmol. 245, 1773–1780.

Leake, P.A., Stakhovskaya, O., Hradek, G.T., Hetherington, A.M., 2008. Factors influencing neurotrophic effects of electrical stimulation in the deafened developing auditory system. Hear. Res. 242, 86–99.

Linden, R., 1994. The survival of developing neurons: a review of afferent control. Neuroscience 58, 671–682.

Macherey, O., van, Wieringen, A., Carlyon, R.P., Deeks, J.M., Wouters, J., 2006. Asymmetric pulses in cochlear implants: effects of pulse shape, polarity, and rate. J. Assoc. Res. Otolaryngol. 7, 253–266.

McCreery, D.B., Agnew, W.F., Yuen, T.G., Bullara, L., 1990. Charge density and charge per phase as cofactors in neural injury induced by electrical stimulation. IEEE Trans. Biomed. Eng. 37, 996–1001.

McCreery, D.B., Agnew, W.F., Yuen, T.G., Bullara, L., 1995. Relationship between stimulus amplitude, stimulus frequency and neural damage during electrical stimulation of sciatic nerve of cat. Med. Biol. Eng. Comput. 33, 426–429.

Mennerick, S., Zorumski, C.F., 2000. Neural activity and survival in the developing nervous system. Mol. Neurobiol. 22, 41–54.

Meyer-Franke, A., Wilkinson, G.A., Kruttgen, A., Hu, M., Munro, E., Hanson Jr., M.G., Reichardt, L.F., Barres, B.A., 1998. Depolarization and cAMP elevation rapidly recruit TrkB to the plasma membrane of CNS neurons. Neuron 21, 681–693.

Miyake, K., Yoshida, M., Inoue, Y., Hata, Y., 2007. Neuroprotective effect of transcorneal electrical stimulation on the acute phase of optic nerve injury. Invest. Ophthalmol. Vis. Sci. 48, 2356–2361.

Morimoto, T., Miyoshi, T., Fujikado, T., Tano, Y., Fukuda, Y., 2002. Electrical stimulation enhances the survival of axotomized retinal ganglion cells in vivo. Neuroreport 13, 227–230.

Morimoto, T., Miyoshi, T., Matsuda, S., Tano, Y., Fujikado, T., Fukuda, Y., 2005. Transcorneal electrical stimulation rescues axotomized retinal ganglion cells by activating endogenous retinal IGF-1 system. Invest. Ophthalmol. Vis. Sci. 46, 2147–2155.

Morimoto, T., Fujikado, T., Choi, J.S., Kanda, H., Miyoshi, T., Fukuda, Y., Tano, Y., 2007. Transcorneal electrical stimulation promotes the survival of photoreceptors and preserves retinal function in royal college of surgeons rats. Invest. Ophthalmol. Vis. Sci. 48, 4725–4732.

Nakauchi, K., Fujikado, T., Kanda, H., Kusaka, S., Ozawa, M., Sakaguchi, H., Ikuno, Y., Kamei, M., Tano, Y., 2007. Threshold suprachoroidal–transretinal stimulation current resulting in retinal damage in rabbits. J. Neural Eng. 4, S50–S57.

Okazaki, Y., Morimoto, T., Sawai, H., 2008. Parameters of optic nerve electrical stimulation affecting neuroprotection of axotomized retinal ganglion cells in adult rats. Neurosci. Res. 61, 129–135.

Sato, T., Fujikado, T., Lee, T.S., Tano, Y., 2008a. Direct effect of electrical stimulation on induction of brain-derived neurotrophic factor from cultured retinal Müller cells. Invest. Ophthalmol. Vis. Sci. 49, 4641–4646.

Sato, T., Fujikado, T., Morimoto, T., Matsushita, K., Harada, T., Tano, Y., 2008b. Effect of electrical stimulation on IGF-1 transcription by L-type calcium channels in cultured retinal Müller cells. Jpn. J. Ophthalmol. 52, 217–223.

Sato, T., Lee, T.S., Takamatsu, F., Fujikado, T., 2008c. Induction of fibroblast growth factor-2 by electrical stimulation in cultured retinal Mueller cells. Neuroreport 19, 1617–1621.

Shen, S., Wiemelt, A.P., McMorris, F.A., Barres, B.A., 1999. Retinal ganglion cells lose trophic responsiveness after axotomy. Neuron 23, 285–295.

Udina, E., Furey, M., Busch, S., Silver, J., Gordon, T., Fouad, K., 2008. Electrical stimulation of intact peripheral sensory axons in rats promotes outgrowth of their central projections. Exp. Neurol. 210, 238–247.

Xu, H.P., Zhao, J.W., Yang, X.L., 2002. Expression of voltage-dependent calcium channel subunits in the rat retina. Neurosci. Lett. 329, 297–300.

Yuen, T.G., Agnew, W.F., Bullara, L.A., Jacques, S., McCreery, D.B., 1981. Histological evaluation of neural damage from electrical stimulation: considerations for the selection of parameters for clinical application. Neurosurgery 9, 292–299.

Generation of a Transgenic Rabbit Model of Retinal Degeneration

Mineo Kondo,[1] Takao Sakai,[1] Keiichi Komeima,[1] Yukihide Kurimoto,[1] Shinji Ueno,[1] Yuji Nishizawa,[2] Jiro Usukura,[3] Takashi Fujikado,[4] Yasuo Tano,[5] and Hiroko Terasaki[1]

Purpose. To generate a transgenic (Tg) rabbit model of retinal degeneration and to characterize the pattern of degeneration by using histology and electrophysiology.

Methods. Rhodopsin Pro347Leu Tg rabbits were generated by BAC transgenesis. Tg rabbits were identified by Southern blot analysis, and the expression levels were measured by quantitative RT-PCR. Retinal histology was examined by light and electron microscopy and immunohistochemistry. Retinal function was assessed by full-field electroretinograms (ERGs).

Results. Six lines of Tg rabbits were generated, and two lines with higher levels of expression showed rod-dominant progressive retinal degeneration. Retinal histology indicated a marked regional variation in the loss of photoreceptors with the central retina more severely affected than the peripheral retina. The characteristics of the ERGs of transgenic rabbits indicated that the rod components of the ERGs were reduced to only 5% by 48 weeks, whereas the cone components remained at 35% in the wild-type at the same time point. The retinal ultrastructure of Tg rabbits showed a large number of small vesicles that accumulated in the extracellular space of the photoreceptors.

Conclusions. To the best of the authors' knowledge, this is the first rabbit model of progressive retinal degeneration. Because rabbits have large eyes and are easy to handle and breed, they will provide a useful animal model for the study of the pathophysiology of and new treatments for retinal degeneration. (*Invest Ophthalmol Vis Sci.* 2009;50:1371–1377) DOI:10.1167/iovs.08-2863

Retinitis pigmentosa (RP) is the name given to a group of inherited retinal disorders characterized by a progressive loss of rod and cone photoreceptors and eventual atrophy of the entire retina.[1–3] The worldwide prevalence of RP is approximately 1 in 4000, meaning that more than 1 million individuals are affected worldwide.[3] RP is genetically heterogeneous; mutations in several photoreceptor-specific and some nonspecific genes are known to cause the condition.[4] Of these, mutations in the rhodopsin gene are the most prevalent class identified to date, causing approximately 25% to 40% of the autosomal dominant RP cases.[5,6]

Animal models of RP are important for understanding the pathophysiology and for developing new treatments for these diseases. Various naturally occurring and genetically manipulated animal models of RP have been studied—for example, fruit flies, zebrafish, chickens, mice, rats, cats, dogs, and pigs (for reviews, see Refs. 7, 8). Of these models, midsized and large animal models have become particularly important because their large eyes make it easier to test new treatments. These treatments may include surgical procedures such as intraocular devices,[9,10] subretinal injection of genes for gene therapy,[11] and implantation of retinal prostheses.[12] Several models of retinal degeneration have been identified or generated in cats,[13,14] dogs,[15,16] and pigs,[17] and colonies of affected animals have been established. However, a rabbit model of progressive retinal degeneration has not yet been produced, despite the fact that this animal has large eyes and is easy to breed and handle. In addition, there is a considerable accumulation of past works on the anatomy and physiology of the rabbit eye.[18–21]

Recent advances in the use of bacterial artificial chromosomes (BACs) modified by homologous recombination have promoted the use of this powerful tool in the generation of transgenic (Tg) animals because this technique makes possible the precise and efficient engineering of large DNA fragments.[22–25] In the present study, we used BAC transgenesis to generate a rhodopsin Tg rabbit model of retinal degeneration. These Tg rabbits exhibited rod-dominant, progressive photoreceptor degeneration and striking regional variation in the pattern of photoreceptor loss.

Methods

This study was conducted in accordance with the ARVO Statement for the Use of Animals in Ophthalmic and Vision Research. All protocols were approved by the Institutional Review Board of the Nagoya University Graduate School of Medicine.

Rabbit Rhodopsin BAC Clone

The rabbit rhodopsin BAC clone, LB1-7M22, was selected from the LBNL-1 New Zealand White Rabbit BAC library by hybridization of high-density arrayed nylon filters using a probe that consisted of a [P^{32}]-labeled fragment of exon 5 of the rabbit rhodopsin gene. The clone was obtained from the BACPAC Resources Center at the Children's Hospital of Oakland Research Institute. The presence of a full-length rabbit rhodopsin genomic sequence was verified by Southern blot analysis with a probe that consisted not only of exon 4 of the rhodopsin gene but also exon 14 of the rabbit *WDR10* gene and exon 25 of the rabbit *PLXND1* gene. These latter two genes are the 5′- and 3′-flanking genes, respectively, of the rabbit rhodopsin gene (Fig. 1A). The exon 4 genomic fragment of the rabbit rhodopsin gene, exon 14

From the [1]Department of Ophthalmology, Graduate School of Medicine, and the [3]Department of Materials Physics and Engineering, Graduate School of Engineering, Nagoya University, Nagoya, Japan; the [2]Research Institute of Life and Health Sciences, Chubu University, Kasugai, Japan; and the Departments of [4]Applied Visual Science and [5]Ophthalmology, Graduate School of Medicine, Osaka University, Suita, Japan.

Supported by Health Sciences Research Grant H16-sensory-001 from the Ministry of Health, Labor, and Welfare of Japan, and Grants 18591913 and 18390466 from the Ministry of Education, Culture, Science, and Technology of Japan.

Submitted for publication September 12, 2008; revised November 9, 2008; accepted January 2, 2009.

Disclosure: **M. Kondo**, None; **T. Sakai**, None; **K. Komeima**, None; **Y. Kurimoto**, None; **S. Ueno**, None; **Y. Nishizawa**, None; **J. Usukura**, None; **T. Fujikado**, None; **Y. Tano**, None; **H. Terasaki**, None

The publication costs of this article were defrayed in part by page charge payment. This article must therefore be marked "*advertisement*" in accordance with 18 U.S.C. §1734 solely to indicate this fact.

Corresponding author: Mineo Kondo, Department of Ophthalmology, Nagoya University Graduate School of Medicine, 65 Tsuruma-cho, Showa-ku, Nagoya 466-8550, Japan; kondomi@med.nagoya-u.ac.jp.

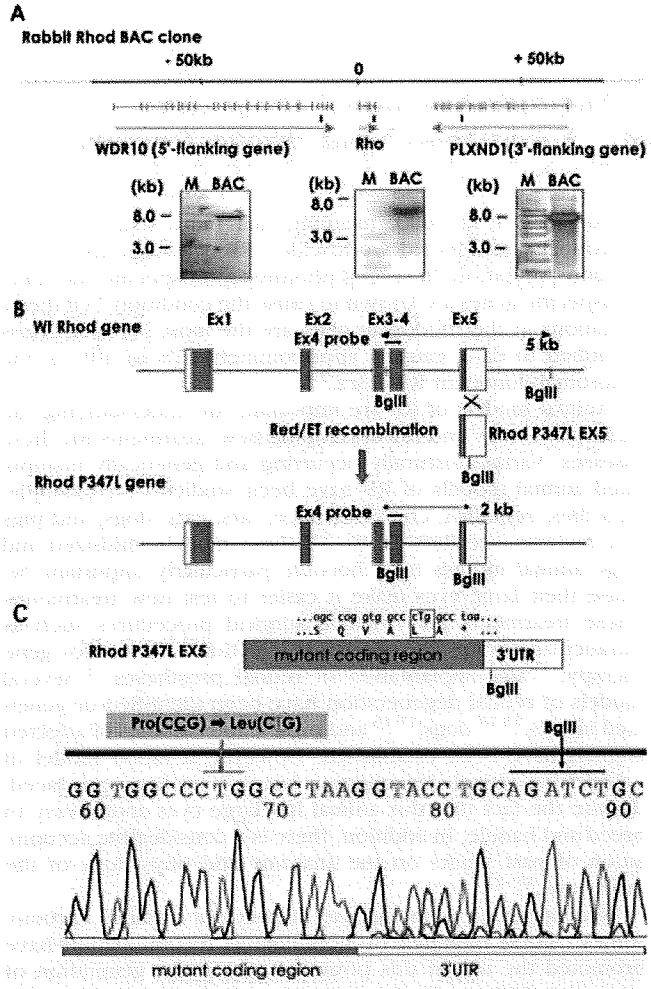

FIGURE 1. Rhodopsin P347L BAC construction by recombineering. (A) Presumed structure of the rabbit rhodopsin BAC clone. The BAC clone contains the full-length rabbit rhodopsin genomic sequence, as determined by Southern hybridization probed by the 5′-flanking gene (*left*), rhodopsin gene (*middle*), and 3′-flanking gene (*right*). *Underbars*: positions of the Southern hybridization probes used. (B) The transgene construct. The sequence of exon 5 of the WT rhodopsin gene (*top*) was replaced by the rhodopsin P347L exon 5 sequence (*middle*) by Red/ET recombination. The rhodopsin P347L gene (*bottom*) has a *Bgl*II restriction site for Tg. (C) Sequence analysis for the rhodopsin P347L mutation. The rhodopsin P347L exon 5 fragment was amplified from the rhodopsin P347L BAC construct by PCR and sequenced.

of the rabbit *WDR10* gene, and exon 25 of the rabbit *PLXND1* gene were amplified by PCR and subcloned into the pGEM-T easy vector (Promega, Madison, WI) for labeling with [P^{32}].

BAC Tg Construct

A rhodopsin P347L BAC Tg construct harboring a C-to-T transition in exon 5 of the rabbit rhodopsin gene was generated by BAC recombineering (Fig. 1B). A point mutation was introduced into the rabbit rhodopsin BAC clone.[24] In brief, an rpsL-neo counter selection cassette, flanked by 40-nucleotide homologous arm sequences on either side of the C-to-T transition site of the rhodopsin gene, was amplified by PCR. The amplified rpsL-neo counter selection cassette was inserted into the rhodopsin gene of the rabbit BAC clone by Red/ET recombination. The subcloned exon 5 fragment of the rabbit rhodopsin gene was modified with a C-to-T transition at proline 347, and the serial restriction sites *Kpn*I, *Pst*I, and *Bgl*II in the 3′-untranslated region. The modified sequence was subcloned into the pGEM-T easy vector for sequencing. The rpsL-neo cassette inserted into the rhodopsin gene of the rabbit BAC clone was replaced by the modified exon 5 fragment by using rpsL counter selection. The BAC modification was verified by Southern blot analysis and sequencing (Fig. 1C). The rhodopsin P347L BAC transgene was purified in a modified procedure.[26] The BAC Tg construct was extracted from 250 mL of *Escherichia coli* culture. For purification, 10 μg of the BAC Tg construct was linearized overnight with PI-*Sce*I endonuclease (New England Biolabs, Beverly, MA), which cleaves a unique site in the BACe3.6 vector sequence. The linearized BAC DNA was separated by pulsed-field gel electrophoresis (PFGE) and extracted from the preparative pulsed-field gel by electroelution. After dialysis against a TE buffer containing 0.1 mM EDTA, aliquots of DNA were subjected to PFGE for size and quality control. The BAC DNA concentration was adjusted to 1 ng/μL for microinjections. The aliquots of BAC DNA solution were stored at 4°C until the microinjections were performed.

Rhodopsin P347L Tg Rabbits

Rhodopsin P347L Tg rabbits were generated by pronuclear injection of the BAC Tg construct into New Zealand White rabbit embryos. Transgenic founders and germline transmission of the BAC Tg construct were assessed by Southern blot analysis of *Bgl*II-digested ear DNA, which was probed with a [P^{32}]-labeled exon 4 fragment of the rabbit rhodopsin gene.

DNA Fluorescence In Situ Hybridization Analysis

DNA FISH analysis was used to examine the actual site of the integrated transgene for each Tg line. Chromosome preparations were obtained with standard techniques and hybridized with a full-length rhodopsin P347L BAC Tg construct as a probe. The probe was labeled with biotin (Roche Diagnostics GmbH, Mannheim, Germany) and detected with avidin-FITC (Fluorescein Avidin D; Vector Labs, Burlingame, CA). The site of the transgene integration was determined by using a standard rabbit chromosome map.[27]

Quantitative RT-PCR

One milligram of total retinal RNA (12 weeks of age) was incubated with 200 units of reverse transcriptase (SuperScript II; Invitrogen, Carlsbad, CA), and the cDNA was used for quantitative RT-PCR (qRT-PCR; QuantiTect SYBR Green PCR Kit; Qiagen, Valencia, CA) and a thermocycler (LightCycler 1.5; Roche Applied Science, Indianapolis, IN). Twenty-microliter reactions were loaded into the thermocycler containing 2 μL of the cDNA sample and 0.5 μM of primers specific for the mutated rhodopsin (forward: 5′-CTA CAT CAT GAT GAA CAA GCA G-3′ and reverse: 5′-TGG CTG GTC TCC GTC TTG GAA-3′) or common primers for wild-type (WT) and mutated rhodopsin (forward: 5′-CTA CAT CAT GAT GAA CAA GCA G-3′ and reverse: 5′-GCA GTG CAG ATC TGC AGG T-3′). For quantification, a standard curve was generated from a cDNA template for each gene. The relative levels of transgene expression were quantified as a ratio of the Tg to the endogenous rhodopsin mRNA.

Clinical Ophthalmic Observations

Ophthalmic examinations were conducted every month after birth. Examinations of the cornea, anterior chamber, iris, and lens were performed by slit-lamp biomicroscopy. The vitreous and retina were examined by indirect ophthalmoscopy. A fundus camera (Kowa, Nagoya, Japan) was used for fundus photography and fluorescein angiography.

Electroretinograms

Animals were dark-adapted for 60 minutes, then anesthetized with ketamine (25 mg/kg, IM) and xylazine (2 mg/kg, IM). ERGs were recorded with Burian-Allen bipolar contact lens electrodes (Hansen Laboratory, Iowa City, IA). The animals were placed in a Ganzfeld bowl and stimulated with stroboscopic stimuli of 2.2 log cd · s · m^{-2}

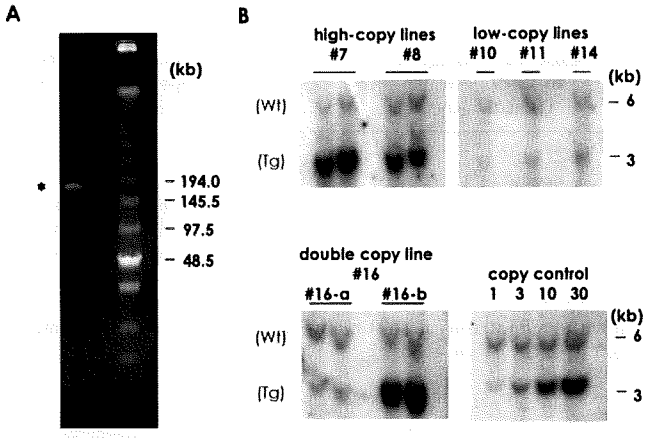

FIGURE 2. Generation of rhodopsin P347L Tg rabbits. (A) Purified rhodopsin P347L transgene construct. PFGE showed that the purified rhodopsin P347L transgene construct was almost 150 kb in size. (B) Southern blot analysis of F1 rabbits of rhodopsin P347L Tg lines. The endogenous rhodopsin WT gene and the rhodopsin P347L transgene were detected as 6 and 3 kb *Bgl*II fragments that hybridized to an exon 4 probe. The copy numbers of the integrated transgene for each line were determined by comparing with a control copy number signal intensity.

(photopic units) maximum intensity. Eight steps of stimulus intensities, ranging from −4.8 to 2.2 log cd · s · m^{-2}, were used for the scotopic ERG recordings, and four steps of stimuli, ranging from −0.8 to 2.2 log cd · s · m^{-2}, were used for the photopic ERGs. The photopic ERGs were recorded on a rod-suppressing white background of 1.3 log cd · m^{-2}. The signals were amplified, bandpass filtered between 0.3 and 1000 Hz, and averaged by a computer-assisted signal analysis system (MEB-9100 Neuropack; Nihon Kohden, Tokyo, Japan). The electrical activities of the rod and cone photoreceptors were assessed by the maximum response of the rod and cone a-waves. The maximum rod a-wave was extracted by waveform subtraction of the photopic ERG from the scotopic ERG at the maximum stimulus intensity of 2.2 log cd · s · m^{-2}.

Rod and cone photoreceptor function was also assessed by the a-wave (P3)-fitting model of Hood and Birch.[28] The a-wave was fitted with the following equation:

$$P3(i, t) = \{1 - \exp[-i \cdot S(t - t_d)^2]\} \cdot Rm \text{ (for } t > t_d)$$

where i is the flash energy (log cd · s · m^{-2}); t_d is the time delay, t is the time after the flash onset, S is the sensitivity, and Rm is maximum response amplitude.

Retinal Histology

Rabbit eyes were fixed overnight in a mixture of 10% neutral buffered formalin and 2.5% glutaraldehyde; F-G fixative), then transferred to 10% neutral buffered formalin. The tissues were trimmed, embedded in paraffin, sectioned vertically through the optic nerve (superior-inferior), and stained with hematoxylin and eosin. The thickness of the outer nuclear layer (ONL) was measured at 10 locations at 2-mm intervals.

Immunohistochemistry

Freshly prepared rabbit eyes were fixed with 4% formaldehyde in phosphate buffer for 2 hours at 4°C. After fixation, the eyes were immersed in 20% sucrose, frozen in OCT compound (Sakura Finetechnical Co., Ltd., Tokyo, Japan), and sectioned at 15 μm. The tissue sections were processed for immunofluorescence staining with anti-rhodopsin antibody (RET-P1; Santa Cruz Biotechnology), followed by Alexa Fluor 488-conjugated anti-mouse IgG and Alexa Fluor 568-conjugated peanut agglutinin (PNA; Invitrogen), a lectin that binds specifically to rabbit cone photoreceptors.[29] Specimens were observed with a fluorescence microscope (BX61 microscope with digital photograph system DP70-BSW; Olympus, Tokyo, Japan).

Electron Microscopy

Eyes were enucleated from anesthetized rabbits (6-week-old WT and line 7 Tg rabbits). The anterior segment was removed, and the retina was fixed in 2.5% glutaraldehyde for 2 hours. After subsequent fixation in 1% osmium tetroxide for 90 minutes, the retina was dehydrated through a graded series of ethanols (50%–100%), and cleared in propylene oxide. Finally, the tissue was embedded in epoxy resin. Ultrathin sections were cut on an ultramicrotome (Ultracut E; Reichert-Jung, Vienna, Austria) and stained with uranyl acetate and lead citrate. The stained sections were observed by transmission electron microscopy (H-7650; Hitachi Co., Tokyo, Japan).

RESULTS

Generation of Tg Rabbits

We identified a rabbit rhodopsin BAC clone that included sequences approximately 150 kb upstream of the transcription initiation codon, the entire rhodopsin structural gene, and sequences downstream of the termination codon of the gene (Fig. 1A). Assuming that these genomic sequences would lead to correct expression of the rhodopsin gene, we inserted a C-to-T transition into the BAC clone in the codon of proline 347 by using BAC recombineering (Fig. 1B). The mutation introduced into the BAC Tg construct was then confirmed by sequence analysis (Fig. 1C). The C-to-T transition in exon 5 of the rabbit rhodopsin gene locus resulted in a proline-to-leucine substitution at codon 347.

After the BAC modification in *E. coli*, the linearized BAC Tg construct was purified and injected into rabbit embryos at the pronucleus stage. PFGE showed that the purified rhodopsin P347L Tg construct was approximately 150 kb (Fig. 2A). Southern blot analysis showed that 12 of 80 newborn rabbits (15%) were transgene positive, and 10 of the 12 survived (Table 1). These 10 founders were bred with WT rabbits, and six founders transmitted the transgene to their offspring.

Characteristics of Each Line of Tg Rabbit

FISH analysis showed that five founders, rabbits 7, 8, 10, 11, and 14, had a single site of transgene integration, and one founder, rabbit 16, had integrations at two sites (Table 2). Three lines, 10, 11, and 14, carried low copy numbers of the transgene, and two lines, rabbits 7 and 8, carried high copy numbers (Fig. 2B). The founder of line 16 carried both high and low copy numbers with transgene insertions on different

TABLE 1. Number of Animals and Zygotes Used to Generate Tg Rabbits

Donor rabbits (total)	36
Zygotes recovered (total)	800
Fertilized zygotes (%)	540 (68)
Zygotes microinjected (%)	456 (84)
Zygotes implanted (%)	456
Zygotes implanted per recipient rabbit (mean ± SD)	27 ± 3
Recipient rabbits	17
Pregnancy rate (%)	12 (71)
Gestation period (days, mean ± SD)	32 ± 1
Rabbits born (total)	80
Transgenic positive (F0) rabbit (surviving)	12 (10)
Founders that passed the transgene onto their offspring	6

TABLE 2. Characteristics of Six Lines of Tg Rabbits

Line	Site of Insertion	Estimated Copy Number	Ratio of Transgene to Endogenous Opsin mRNA	Amplitude of Maximum Scotopic ERG a-Wave at 12 Wk (μV)
7	13q	30	4:1	49.6 ± 12.7 (n = 5)
8	12q	10	1:1	96.5 ± 20.1 (n = 5)
10	2q	1	0.15:1	180.2 (n = 1)
11	Xq	3	0.07:1	165.1 (n = 1)
14	9p	3	0.1:1	159.3 (n = 1)
16*	6q, 3p	Variable	Variable	Variable

Maximum scotopic ERGs (mixed rod and cone response) were measured with high intensity flash stimulus of 2.2 log cd · s · m^{-2}. Results are expressed as the mean ± SD. The a-wave amplitude of WT NZW rabbits was 170 ± 28 μV (n = 5).

* Double copy line.

chromosomes that yielded two different lines, 16a and 16b (Fig. 2B).

The transgene copy number estimated by Southern blot analysis correlated roughly with the level of transgene expression and the degree of photoreceptor degeneration as determined by the ERG a-wave amplitude (Table 2). Lines 7 and 8, which had higher transgene copy numbers, had higher levels of transgene expression and showed a rapid, progressive reduction in the a-wave amplitude. In contrast, lines 10, 11, and 14, which had lower copy numbers, had lower transgene expression levels, and the a-wave amplitude was not significantly different from that of age-matched (12 weeks of age) WT rabbits. The a-wave amplitudes for these three lines remained within the normal range, even at 48 weeks (data not shown).

Because of a restriction in the number of rabbits that could be housed in our animal facilities, we mainly produced and investigated line 7, which had the highest level of transgene expression and the most severe photoreceptor degeneration.

Clinical Findings

Tg rabbits from all lines had normal corneas, anterior chambers, and clear lenses. There was no difference in the fundus appearance or fluorescein angiograms between WT and Tg rabbits at any age up to 40 weeks (Fig. 3). However, it should be noted that Tg animals were on an albino background, and the characteristic bone spicule pigmentation of the retina seen in RP eyes would therefore not be expected.

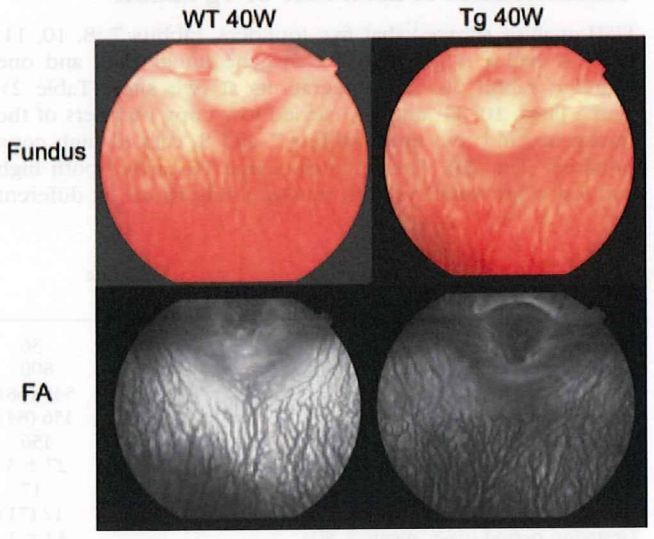

FIGURE 3. Fundus photographs (*top*) and fluorescein angiograms (*bottom*) obtained from a 40-week-old WT and a rhodopsin P347L Tg rabbit from line 7. The appearances of the fundus and the angiogram of the Tg rabbit were indistinguishable from those of the WT rabbit, even at 40 weeks.

Retinal Histology and Immunohistochemistry

Retinal histology in the area of the visual streak, the central area of the rabbit retina, of a WT and a line 7 Tg rabbit at different ages are shown in Figure 4A. At 2 weeks of age, the retinal histology of Tg rabbits was nearly indistinguishable from that of WT rabbits. Both types of rabbits had six or seven layers of nuclei in the ONL. Thereafter, the thickness of the ONL in Tg rabbits progressively decreased (Fig. 4B). At 48 weeks, only a single row of nuclei remained in the ONL of the retina of Tg rabbits. In contrast, the architecture and thickness of the middle and inner retinal layers were relatively well preserved even at 48 weeks of age.

We also examined the retina of Tg rabbits by immunohistochemistry using an anti-rhodopsin antibody and PNA lectin. There was no detectable rhodopsin labeling in the retina of 48-week-old Tg rabbit in the area of the visual streak (Fig. 5). The cone inner and outer segments were stained by PNA, but their structures were severely disrupted in the 48-week-old Tg rabbit.

There were distinct regional differences in the degree of photoreceptor loss in the older Tg rabbits. The retinal sections from 12-week-old WT and Tg rabbits at three locations along the vertical meridian are shown in Figure 4C. It is known that in normal rabbits, the density of rod and cone photoreceptors is highest at the visual streak located inferior to the optic nerve head.[20] Consistent with previous reports, the thickness of the ONL in WT rabbits was at its maximum near the visual streak. In contrast, the ONL in Tg rabbits was thinnest near the visual streak and was relatively preserved in the peripheral retina (Fig. 4D).

ERGs of Tg Rabbits

To evaluate the retinal function of the rod and cone systems of Tg rabbits, we recorded full-field scotopic and photopic ERGs. The scotopic and photopic ERGs elicited by different stimulus intensities from a 12-week-old WT and 12- and 48-week-old Tg rabbits are shown in Figures 6A and 6B, respectively. Compared with the ERGs recorded from 12-week-old WT rabbits, the ERG amplitudes of Tg rabbits were clearly reduced at 12 weeks, and the degree of reduction became more severe at 48 weeks. The amplitude of the maximum rod a-wave, which reflects rod photoreceptor activity, was 28% of the WT at 12 weeks and reduced to 5% at 48 weeks (Fig. 6C). In contrast, the maximum cone a-wave amplitude was 65% of the WT at 12 weeks and remained at 35% even at 48 weeks (Fig. 6D). The a-wave fitting model of Hood and Birch[28] also revealed that not only the maximum response amplitude (Rm), but also the transduction sensitivity (S) were abnormal in both rod and

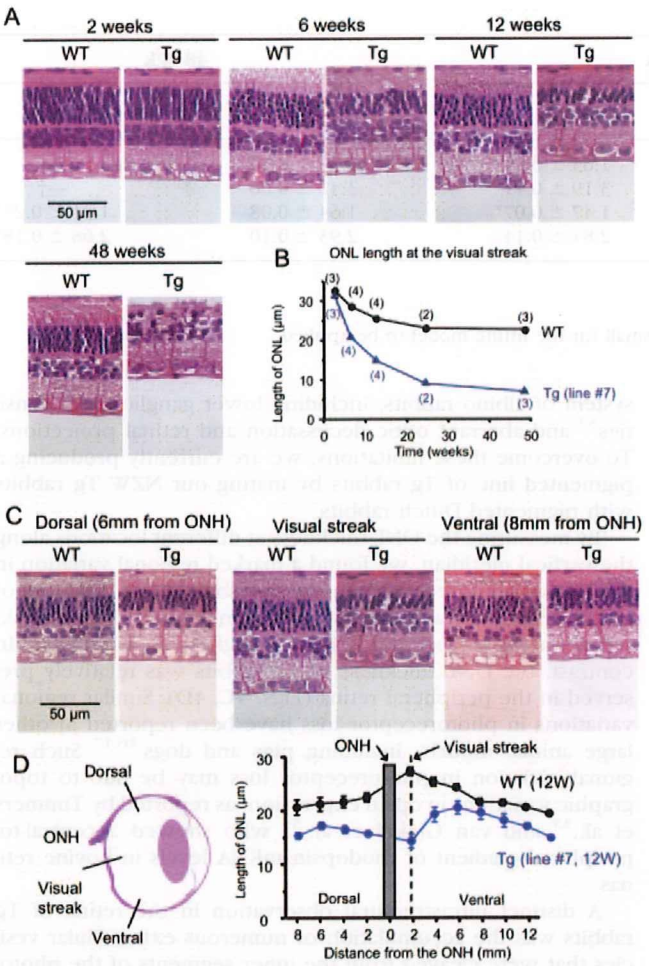

FIGURE 4. Retinal histology of Tg rabbits (line 7). **(A)** Retinal sections of WT and Tg rabbits at 2, 6, 12, and 48 weeks of age. **(B)** Changes in the thickness of the ONL at different ages (in weeks) for WT and Tg rabbits. The number of animals examined is shown in parentheses. **(C)** Vertical retinal sections 6 mm superior to the optic nerve head (ONH), at the visual streak, and 8 mm inferior to the ONH of 12-week-old WT and Tg rabbits. **(D)** Thickness of the ONL along the vertical meridian measured at 10 retinal locations at 2-mm intervals. Mean ± SEM of five WT and five Tg rabbits are plotted.

cone photoreceptors of Tg rabbits (Table 3). These results indicated a rod-dominant, progressive photoreceptor dysfunction in the retina of this line of Tg rabbits.

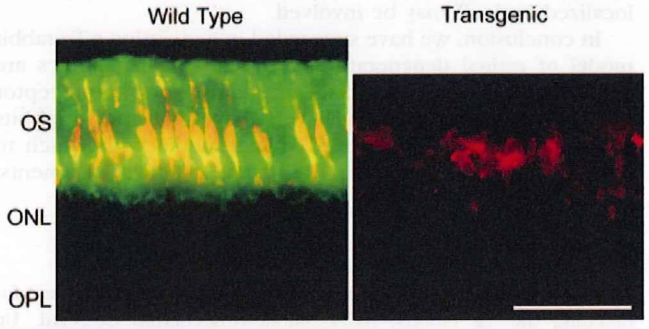

FIGURE 5. Immunohistochemical analysis of rod and cone photoreceptors double labeled with rhodopsin (*green*) and PNA (*red*) at the visual streak of 48-week-old WT (*left*) and transgenic (*right*) rabbits. Bar, 50 µm.

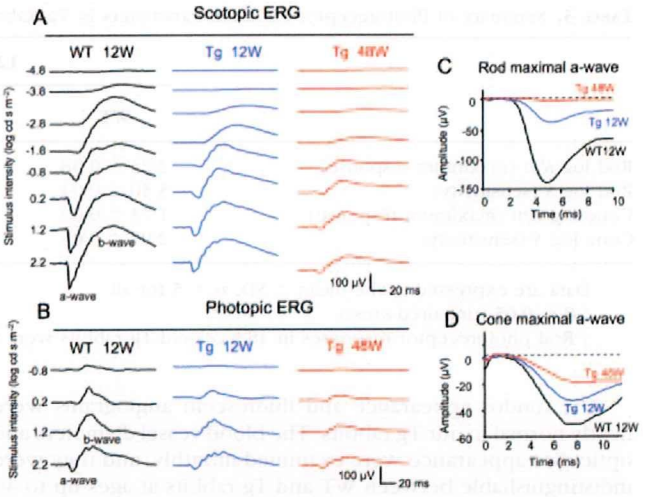

FIGURE 6. ERGs recorded from 12-week-old WT and 12- and 48-week-old rhodopsin P347L (line 7) Tg rabbits. **(A)** Scotopic ERGs elicited by eight different stimulus intensities. **(B)** Photopic ERGs elicited by four different stimulus intensities. **(C)** Rod maximum a-waves elicited by 2.2 log cd · s · m^{-2}. These responses were obtained by waveform subtraction of photopic ERGs from scotopic ERGs. **(D)** Cone maximum a-waves elicited by 2.2 log cd · s · m^{-2} on a rod-suppressing white background of 1.3 log cd · s · m^{-2}.

Presence of Extracellular Vesicles in the Tg Rabbit Retina

Finally, we compared the retinal ultrastructure of 6-week-old WT and line 7 Tg rabbits. The outer segments of the photoreceptors were slightly shorter and less organized in the retinas of 6-week-old Tg rabbits, although the outer segments still contained many well-packed discs at this age (Fig. 7A).

A striking finding in the Tg rabbit retina was the large number of small vesicles that accumulated in the extracellular space of the photoreceptors (Fig. 7A, asterisks). The vesicles were 50 to 300 nm in size and bound to a single membrane. We also found that these vesicles were cleaved from the membranes of the inner segments of the photoreceptors (Fig. 7B, arrows).

DISCUSSION

The purpose of this study was to generate a rabbit model of progressive retinal degeneration and to characterize the pattern of degeneration by using histology and electrophysiology. For this purpose, we used rabbit BAC transgenesis, which permitted us to produce a point mutation with no effect on the rest of the large rhodopsin gene, including the regulatory regions of the rhodopsin gene.[22–24] BAC transgenesis is known to provide high tissue- and stage-specific transgene expression that is independent of the site of integration and dependent on the number of integrated copies.[25]

We succeeded in generating six lines of Tg rabbits with different expression levels. Two lines showed high transgene expression levels and progressive retinal degeneration. Retinal histologic and ERG studies showed early loss of rod function associated with relatively preserved cone function, which is very similar to the clinical findings of human RP patients with the rhodopsin P347L mutation.[30,31] To the best of our knowledge, this is the first rabbit model of progressive retinal degeneration. Because rabbits have large eyes and are easy to handle and breed, we believe that our Tg rabbits are useful animal models for testing various new treatments, including surgical procedures.

TABLE 3. Summary of Photoreceptor Function Parameters in Tg Rabbits

	12 Wk		48 Wk	
	WT	Tg	WT	Tg
Rod log *Rm* (maximum response)	2.23 ± 0.08	1.63 ± 0.06*	2.06 ± 0.10	—†
Rod log *S* (sensitivity)	3.50 ± 0.04	3.19 ± 0.11*	3.42 ± 0.06	—†
Cone log *Rm* (maximum response)	1.73 ± 0.09	1.47 ± 0.07*	1.64 ± 0.08	1.21 ± 0.23*
Cone log *S* (sensitivity)	2.97 ± 0.05	2.84 ± 0.14	2.93 ± 0.10	2.68 ± 0.18*

Data are expressed as the mean ± SD. $n = 5$ for all.
* $P < 0.05$ (unpaired *t*-test).
† Rod photoreceptor responses in 48-week-old Tg rabbits were too small for the fitting model to be applied.

The fundus appearance and fluorescein angiograms were nearly normal in our Tg rabbits. The blood vessel diameters and optic disc appearance were examined monthly, and they were indistinguishable between WT and Tg rabbits at ages up to 40 weeks. An early sign of RP in human patients is an attenuation of blood vessel diameters in the eye. The normal diameter of the retinal vessels in our Tg rabbits may be due to the characteristics of rabbit retina, because retinal vessels in rabbits are confined to the horizontal myelinated bands, comprising optic axons, oligodendrocytes, and astrocytes, and are not associated with the inner retinal layers, as in vascular retinas.

In this study, we generated the transgenic rabbits on an albino background (NZW), because the rabbit BAC library was available only for NZW rabbits. However, this albino background may limit the model's usefulness. First, normal fundus coloring without any pigmentation in our Tg rabbits may have occurred because we used the nonpigmented NZW rabbits. Second, it is known that there are other anomalies in the visual system of albino rabbits, including lower ganglion cell densities[32] and aberrant optic decussation and retinal projections. To overcome these limitations, we are currently producing a pigmented line of Tg rabbits by mating our NZW Tg rabbits with pigmented Dutch rabbits.

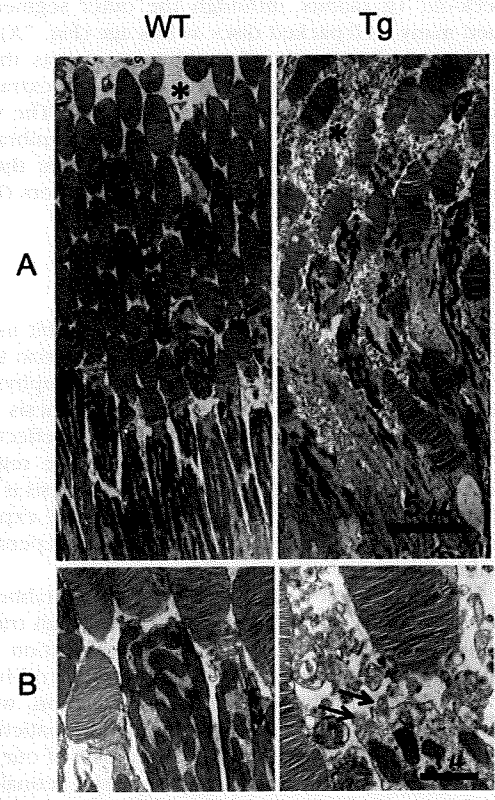

FIGURE 7. Ultrastructural analyses of 6-week-old WT (*left*) and Tg (*right*) rabbit retinas. (**A**) Tg rabbit retina showing many small vesicles accumulated in the extracellular space (*). (**B**) These abnormal vesicles were cleaved from the inner segment of photoreceptors (*arrows*).

By measuring the ONL thickness at different locations along the vertical meridian, we found a marked regional variation in the loss of photoreceptors in the Tg rabbit retina. The loss of photoreceptors was at its maximum near the visual streak, where the photoreceptor density is highest in WT rabbits. In contrast, the ONL thickness in Tg rabbits was relatively preserved in the peripheral retina (Figs. 4C, 4D). Similar regional variations in photoreceptor loss have been reported in other large animal models, including pigs and dogs.[16,17] Such regional variation in photoreceptor loss may be due to topographic variations in opsin expression, as reported by Timmers et al.,[33] and van Ginkel et al.,[34] who showed a central-to-peripheral gradient of rhodopsin mRNA levels in bovine retinas.

A distinct ultrastructural observation in the retina of Tg rabbits was the accumulation of numerous extracellular vesicles that were cleaved from the inner segments of the photoreceptors. At this stage, the outer segments still contained well-packed discs. These findings are consistent with findings in Tg mice with the P347S rhodopsin mutation.[35] Using two monoclonal antibodies against rhodopsin, Li et al.[35] demonstrated that these small vesicles contain rhodopsin, and they proposed that they were produced as a consequence of a defect in the transport of rhodopsin from the inner segment to the disc membranes of the outer segments. Although we have not yet examined whether the vesicles contain rhodopsin in our Tg rabbits, the similarity in the ultrastructural findings and site of rhodopsin mutation suggested that the defective delivery of opsin to the outer segment may be one of the causes of photoreceptor cell death in our Tg rabbits. However, other factors, including an overexpression of rhodopsin,[36,37] prolonged activation of phototransduction,[38] or activation of mislocalized opsin,[39] may be involved.

In conclusion, we have succeeded in generating a Tg rabbit model of retinal degeneration. Although further studies are needed to determine the exact mechanism of photoreceptor death observed in our model, we believe that our Tg rabbits will serve as a useful midsized animal model with which to study the pathophysiology of RP and develop novel treatments.

Acknowledgments

The authors thank Kensaku Kitada (Kitayama Labes Co., Ina, Japan) for breeding the Tg rabbits; Akira Shiota (PhoenixBio Co., Ltd. Utsunomiya, Japan) for technical help with BAC transgenesis; Robert E. Marc and Bryan W. Jones of Utah University for critical comments on the manuscript; and Duco I. Hamasaki of Miami University and Yozo Miyake of Shukutoku University for discussions of the manuscript.

References

1. Heckenlively JR. RP syndromes. In: Heckenlively JR, ed. *Retinitis Pigmentosa.* Philadelphia: JB Lippincott; 1988:221-252.
2. Weleber RG, Gregory-Evance K. Retinitis pigmentosa and allied disorders. In: Hinton DR, ed. *Basic Science and Inherited Retinal Disease: Retina.* Vol. 1, 4th ed. St. Louis: Mosby; 2006:395-498.
3. Hartong DT, Berson EL, Dryja TP. Retinitis pigmentosa. *Lancet.* 2006;368:1795-1809.
4. Daiger SP, Bowne SJ, Sullivan LS. Perspective on genes and mutations causing retinitis pigmentosa. *Arch Ophthalmol.* 2007;125:151-158.
5. Gal A, Apfelstedt-Sylla E, Janecke AR, Zrenner E. Rhodopsin mutations in inherited retinal dystrophies and dysfunctions. *Prog Retin Eye Res.* 1997;16:51-79.
6. Dryja TP, Hahn LB, Cowley GS, et al. Mutation spectrum of the rhodopsin gene among patients with autosomal dominant retinitis pigmentosa. *Proc Natl Acad Sci USA.* 1991;88:9370-9374.
7. Petersen-Jones SM. Animal models of human retinal dystrophies. *Eye.* 1998;12:566-570.
8. Chader GJ. Animal models in research on retinal degenerations: past progress and future hope. *Vision Res.* 2002;42:393-399.
9. Tao W, Wen R, Goddard MB, et al. Encapsulated cell-based delivery of CNTF reduces photoreceptor degeneration in animal models of retinitis pigmentosa. *Invest Ophthalmol Vis Sci.* 2002;43:3292-3298.
10. Bush RA, Lei B, Tao W, et al. Encapsulated cell-based intraocular delivery of ciliary neurotrophic factor in normal rabbit: dose-dependent effects on ERG and retinal histology. *Invest Ophthalmol Vis Sci.* 2004;45:2420-2430.
11. Acland GM, Aguirre GD, Ray J, et al. Gene therapy restores vision in a canine model of childhood blindness. *Nat Genet.* 2001;28:92-95.
12. Güven D, Weiland JD, Fujii G, et al. Long-term stimulation by active epiretinal implants in normal and RCD1 dogs. *J Neural Eng.* 2005;2:S65-73.
13. Narfström K. Hereditary progressive retinal atrophy in the Abyssinian cat. *J Hered.* 1983;74:273-276.
14. Menotti-Raymond M, David VA, Schäffer AA, et al. Mutation in CEP290 discovered for cat model of human retinal degeneration. *J Hered.* 2007;98:211-220.
15. Acland GM, Fletcher RT, Gentleman S, et al. Non-allelism of three genes (rcd1, rcd2 and erd) for early-onset hereditary retinal degeneration. *Exp Eye Res.* 1989;49:983-998.
16. Kijas JW, Cideciyan AV, Aleman TS, et al. Naturally occurring rhodopsin mutation in the dog causes retinal dysfunction and degeneration mimicking human dominant retinitis pigmentosa. *Proc Natl Acad Sci USA.* 2002;99:6328-6333.
17. Petters RM, Alexander CA, Wells KD, et al. Genetically engineered large animal model for studying cone photoreceptor survival and degeneration in retinitis pigmentosa. *Nat Biotechnol.* 1997;15:965-970.
18. Marc RE. Neurochemical stratification in the inner plexiform layer of the vertebrate retina. *Vision Res.* 1986;26:223-238.
19. Vaney DI, Young HM, Gynther IC. The rod circuit in the rabbit retina. *Vis Neurosci.* 1991;7:141-154.
20. Famiglietti EV, Sharpe SJ. Regional topography of rod and immunocytochemically characterized "blue" and "green" cone photoreceptors in rabbit retina. *Vis Neurosci.* 1995;12:1151-1175.
21. Rockhill RL, Daly FJ, MacNeil MA, et al. The diversity of ganglion cells in a mammalian retina. *J Neurosci.* 2002;22:3831-3843.
22. Yang XW, Model P, Heintz N. Homologous recombination based modification in Escherichia coli and germline transmission in transgenic mice of a bacterial artificial chromosome. *Nat Biotechnol.* 1997;15:859-865.
23. Zhang Y, Buchholz F, Muyrers JP, Stewart AF. A new logic for DNA engineering using recombination in Escherichia coli. *Nat Genet.* 1998;20:123-128.
24. Muyrers JP, Zhang Y, Benes V, et al. Point mutation of bacterial artificial chromosomes by ET recombination. *EMBO Rep.* 2000;1:239-243.
25. Giraldo P, Montoliu L. Size matters: use of YACs, BACs and PACs in transgenic animals. *Transgenic Res.* 2001;10:83-103.
26. Abe K, Hazama M, Katoh H, et al. Establishment of an efficient BAC transgenesis protocol and its application to functional characterization of the mouse Brachyury locus. *Exp Anim.* 2004;53:311-320.
27. Committee for Standardized Karyotype of Oryctolagus Cuniculus. Standard karyotype of the laboratory rabbit, Oryctolagus cuniculus. *Cytogenet Cell Genet.* 1981;31:240-248.
28. Hood DC, Birch DG. Rod phototransduction in retinitis pigmentosa: estimation and interpretation of parameters derived from the rod a-wave. *Invest Ophthalmol Vis Sci.* 1994;35:2948-2961.
29. Blanks JC, Johnson LV. Specific binding of peanut lectin to a class of retinal photoreceptor cells: a species comparison. *Invest Ophthalmol Vis Sci.* 1984:25;546-557.
30. Oh KT, Longmuir R, Oh DM, Stone EM, et al. Comparison of the clinical expression of retinitis pigmentosa associated with rhodopsin mutations at codon 347 and codon 23. *Am J Ophthalmol.* 2003;136:306-313.
31. Berson EL, Rosner B, Sandberg MA, et al. Ocular findings in patients with autosomal dominant retinitis pigmentosa and rhodopsin, proline-347-leucine. *Am J Ophthalmol.* 1991;111:614-623.
32. Oyster CW, Takahashi ES, Fry KR, Lam DM. Ganglion cell density in albino and pigmented rabbit retinas labeled with a ganglion cell-specific monoclonal antibody. *Brain Res.* 1987:425;25-33.
33. Timmers AM, Wintjes ET, Hauswirth WW. Fetal topography of bovine rhodopsin mRNA suggests retinotopographically determined gene expression. *Invest Ophthalmol Vis Sci.* 1995;36:2008-2019.
34. van Ginkel PR, Timmers AM, Szél A, Hauswirth WW. Topographical regulation of cone and rod opsin genes: parallel, position dependent levels of transcription. *Brain Res Dev Brain Res.* 1995;89:146-149.
35. Li T, Snyder WK, Olsson JE, Dryja TP. Transgenic mice carrying the dominant rhodopsin mutation P347S: evidence for defective vectorial transport of rhodopsin to the outer segments. *Proc Natl Acad Sci USA.* 1996;93:14176-14181.
36. Olsson JE, Gordon JW, Pawlyk BS, et al. Transgenic mice with a rhodopsin mutation (Pro23His): a mouse model of autosomal dominant retinitis pigmentosa. *Neuron.* 1992;9:815-830.
37. Tan E, Wang Q, Quiambao AB, et al. The relationship between opsin overexpression and photoreceptor degeneration. *Invest Ophthalmol Vis Sci.* 2001;42:589-600.
38. Chen J, Makino CL, Peachey NS, Baylor DA, Simon MI. Mechanisms of rhodopsin inactivation in vivo as revealed by a COOH-terminal truncation mutant. *Science.* 1995;267:374-377.
39. Alfinito PD, Townes-Anderson E. Activation of mislocalized opsin kills rod cells: a novel mechanism for rod cell death in retinal disease. *Proc Natl Acad Sci USA.* 2002;99:5655-5660.